Cellular/Molecular

Tmc1 Point Mutation Affects Ca^{2+} Sensitivity and Block by Dihydrostreptomycin of the Mechanoelectrical Transducer Current of Mouse Outer Hair Cells

Laura F. Corns,[1] Stuart L. Johnson,[1] Corné J. Kros,[2,3] and Walter Marcotti[1]

[1]Department of Biomedical Science, University of Sheffield, Sheffield, South Yorkshire S10 2TN, United Kingdom, [2]Sussex Neuroscience, School of Life Sciences, University of Sussex, Falmer, Brighton BN1 9QG, United Kingdom, and [3]Department of Otorhinolaryngology, University Medical Center Groningen, University of Groningen, 9700 RB Groningen, The Netherlands

The transduction of sound into electrical signals depends on mechanically sensitive ion channels in the stereociliary bundle. The molecular composition of this mechanoelectrical transducer (MET) channel is not yet known. Transmembrane channel-like protein isoforms 1 (TMC1) and 2 (TMC2) have been proposed to form part of the MET channel, although their exact roles are still unclear. Using *Beethoven* (*Tmc1*$^{Bth/Bth}$) mice, which have an M412K point mutation in TMC1 that adds a positive charge, we found that Ca^{2+} permeability and conductance of the MET channel of outer hair cells (OHCs) were reduced. *Tmc1*$^{Bth/Bth}$ OHCs were also less sensitive to block by the permeant MET channel blocker dihydrostreptomycin, whether applied extracellularly or intracellularly. These findings suggest that the amino acid that is mutated in *Bth* is situated at or near the negatively charged binding site for dihydrostreptomycin within the permeation pore of the channel. We also found that the Ca^{2+} dependence of the operating range of the MET channel was altered by the M412K mutation. Depolarization did not increase the resting open probability of the MET current of *Tmc1*$^{Bth/Bth}$ OHCs, whereas raising the intracellular concentration of the Ca^{2+} chelator BAPTA caused smaller increases in resting open probability in *Bth* mutant OHCs than in wild-type control cells. We propose that these observations can be explained by the reduced Ca^{2+} permeability of the mutated MET channel indirectly causing the Ca^{2+} sensor for adaptation, at or near the intracellular face of the MET channel, to become more sensitive to Ca^{2+} influx as a compensatory mechanism.

Key words: **adaptation; calcium; development; hair cell; mechanotransduction; TMC1**

Significance Statement

In the auditory system, the hair cells convert sound-induced mechanical movement of the hair bundles atop these cells into electrical signals through the opening of mechanically gated ion channels at the tips of the bundles. Although the nature of these mechanoelectrical transducer (MET) channels is still unclear, recent studies implicate transmembrane channel-like protein isoform 1 (TMC1) channels in the mammalian cochlea. Using a mutant mouse model (*Beethoven*) for progressive hearing loss in humans (DFNA36), which harbors a point mutation in the *Tmc1* gene, we show that this mutation affects the MET channel pore, reducing its Ca^{2+} permeability and its affinity for the permeant blocker dihydrostreptomycin. A number of phenomena that we ascribe to Ca^{2+}-dependent adaptation appear stronger, in compensation for the reduced Ca^{2+} entry.

Introduction

The sense of hearing relies on the transduction of sound stimuli into electrical signals, which is performed by mechanically gated ion channels located at the tips of the shorter stereocilia (Beurg et al., 2009). Stereocilia are specialized microvilli forming staircase-like structures, the hair bundles, that project from the upper surface of hair cells. The stereocilia within a hair bundle are

Received June 25, 2015; revised Nov. 5, 2015; accepted Nov. 13, 2015.

Author contributions: L.F.C., C.J.K., and W.M. designed research; L.F.C., S.L.J., and W.M. performed research; L.F.C., C.J.K., and W.M. analyzed data; L.F.C., C.J.K., and W.M. wrote the paper.

This work was supported by Wellcome Trust Grant 102892 (W.M.). C.J.K. is supported by Medical Research Council Grant MR/K005561.

The authors declare no competing financial interests.

This article is freely available online through the *J Neurosci* Author Open Choice option.

Correspondence should be addressed to Walter Marcotti, Department of Biomedical Science, Centre for Sensory Neuroscience, Alfred Denny Building, University of Sheffield, Sheffield, South Yorkshire S10 2TN, UK. E-mail: w.marcotti@sheffield.ac.uk.

DOI:10.1523/JNEUROSCI.2439-15.2016

interconnected by extracellular linkages, the most important of which for the purpose of mechanoelectrical transduction is the tip link (Pickles et al., 1984; Assad et al., 1991; Goodyear et al., 2005). Tip links connect the stereocilia in the direction of optimal mechanical sensitivity, enabling them to transmit force to the mechanoelectrical transducer (MET) channels during bundle displacement, thus modulating their open probability. Although the molecular identity of the MET channel is still uncertain, recent studies have identified two molecules (TMHS/LHFPL5 and TMIE) that are implicated in mechanoelectrical transduction and directly interact with protocadherin-15 (PCDH15), which connects the lower end of the tip link into the stereociliary top (Xiong et al., 2012; Zhao et al., 2014). However, neither of these proteins appears to be the pore-forming subunit of the MET channel (Xiong et al., 2012; Zhao et al., 2014). TMC1 and TMC2 are localized at the tips of the shorter stereocilia (Kurima et al., 2015), the site for mechanoelectrical transduction, and are candidate subunits of the MET channel (Kawashima et al., 2011; Pan et al., 2013). However, recent reports have provided some evidence for a more accessory subunit role for both TMC1 and TMC2, mainly based on the fact that a mechano-gated current could still be elicited in TMC1/TMC2 double knock-outs (Beurg et al., 2014). However, this undefined mechano-gated current can also be elicited in hair cells from normal mice in the absence of tip links and has biophysical and pharmacological properties that are somewhat distinct from those of the MET channel (Marcotti et al., 2014). If this anomalous mechano-gated channel is indeed the MET channel precursor in cochlear hair cells, then TMC1 and TMC2 could be required to make a functionally mature channel pore and/or vestibule facing the extracellular side of the channel.

The *Beethoven* (*Bth*) mutant mouse is a model for progressive hearing loss (DFNA36) caused by a single dominant missense mutation of a methionine to a lysine at position 412 of *TMC1* (Kurima et al., 2002; Vreugde et al., 2002; Nakanishi et al., 2014). In this study, we have used the *Beethoven* mouse and a double-mutant *Beethoven*/*Tmc2* mouse model to provide additional evidence for a direct role of TMC1 and TMC2 in mechanoelectrical transduction in mouse outer hair cells (OHCs). Our results indicate that the M412K point mutation in *Beethoven* mice reduces the permeability of the MET channel for Ca^{2+} and the permeant blocker dihydrostreptomycin (DHS). The *Bth* mutation also abolished the normally observed increase of the resting MET current on OHC depolarization. Increasing the extracellular concentration from its endolymphatic concentration of ~0.04 to 0.1 mM or decreasing intracellular Ca^{2+} buffering caused a decrease in resting open probability of the MET current in *Bth* mutant OHCs but not in wild-type controls. We argue that these observations can be most parsimoniously explained by assuming that the reduced Ca^{2+} permeability indirectly causes the Ca^{2+} sensor for adaptation of the MET channel to become more sensitive to Ca^{2+} influx.

Materials and Methods

Animals and genotyping. All experiments were performed in accordance with Home Office regulations under the Animals (Scientific Procedures) Act 1986 and following approval by the University of Sheffield Ethical Review Committee. The *Beethoven* ($Tmc1^{Bth/+}$ and $Tmc1^{Bth/Bth}$) mice were maintained on a C3HeB/FeJ background. $Tmc1^{Bth}$ encodes a point mutation at residue 412 that is predicted to cause a methionine to lysine substitution (Vreugde et al., 2002). *Tmc2* knock-out mice were obtained from The Jackson Laboratory (B6.129–$Tmc2^{tm1.1Ajg}$). *Beethoven* and $Tmc2^{-/-}$ mice were genotyped as described previously (Marcotti et al., 2006; Pan et al., 2013, respectively). The *Beethoven* mice were obtained from Karen Steel (Kings College, London, UK).

Tissue preparation. OHCs were studied in acutely dissected organs of Corti from postnatal day 2 (P2) to P12. Mice of either sex were killed by cervical dislocation, the cochlea removed, and the organ of Corti dissected in the extracellular solution composed of the following (in mM): 135 NaCl, 5.8 KCl, 1.3 $CaCl_2$, 0.9 $MgCl_2$, 0.7 NaH_2PO_4, 5.6 D-glucose, 10 HEPES-NaOH, and 2 Na-pyruvate. Amino acids and vitamins (Eagle's MEM) were also added from concentrates (pH 7.5; osmolality, 308 mOsmol/kg). The dissected apical and basal coils of the organ of Corti were transferred to a microscope chamber containing extracellular solution and viewed through a long-working-distance 63× water-immersion objective on a Leica DMLFS microscope.

Whole-cell patch clamp. MET currents were recorded at room temperature (20–25°C) using an Optopatch amplifier (Cairn Research). Patch pipettes, with resistances of 2–4 MΩ, were pulled from soda glass capillaries, and the shank of the electrode was coated with surf wax (Mr. Zoggs Sex Wax). For most experiments, except those measuring Ca^{2+} selectivity, pipettes were filled with an intracellular solution composed of the following (in mM): 106 L-glutamic acid, 20 CsCl, 10 Na_2-phosphocreatine, 3 $MgCl_2$, 1 EGTA-CsOH, 5 Na_2ATP, 5 HEPES, and 0.3 GTP (adjusted to pH 7.28 with 1 M CsOH; osmolality, 294 mOsmol/kg). Data acquisition was performed using pClamp software (Molecular Devices) using a Digidata 1440A. Data were filtered at 5 kHz (eight-pole Bessel). Offline data analysis was performed using Origin software (OriginLab). Membrane potentials were corrected for a liquid junction potential of −11 mV measured between electrode and bath solution.

Hair bundle stimulation. MET currents were elicited using a fluid jet from a pipette driven by a 25-mm-diameter piezoelectric disc (Kros et al., 1992; Corns et al., 2014). The fluid jet was preferred to a rigid probe (Peng et al., 2013) because it does not require any previous contact with the hair bundle, which could affect their resting position, and provides a more homogeneous displacement of stereocilia within a bundle compared with the stiff probe (Corns et al., 2014; Nam et al., 2015). The distance of the pipette tip from the bundle was adjusted to elicit a maximal MET current. Mechanical stimuli were applied as steps or saturating 50 Hz sinusoids (filtered at 1 kHz, eight-pole Bessel). Hair bundle motion during fluid jet stimulation was quantified by projecting an image of the OHC bundle onto a pair of photodiodes (LD 2–5; Centronics) at 360× magnification (Corns et al., 2014). This procedure is difficult to perform during MET recordings because it requires optimal orientation of the preparation to produce a bright bundle. Therefore, bundle displacement was not routinely calibrated and was converted as reported previously (10 nm/V; Corns et al., 2014) for the standard recording conditions: fluid jet pipette tip with a diameter of 8–10 μm positioned at ~8 μm from the bundles.

Extracellular and intracellular application of the different solutions. The effect of low Ca^{2+} on the MET current was investigated by perfusing the hair bundle with either low-millimolar Ca^{2+} (0.1 mM), which is in the range of the predicted immature endolymphatic Ca^{2+} (Johnson et al., 2012), or adult endolymph-like Ca^{2+} (0.04 mM; Bosher and Warren, 1978; Salt et al., 1989). The solution containing 0.1 mM Ca^{2+} was as follows (in mM): 147 NaCl, 5.8 KCl, 0.1 $CaCl_2$, 0.7 NaH_2PO_4, 2 Na-pyruvate, 5.6 D-glucose, and 10 K-HEPES-NaOH, pH 7.5. That with 0.04 mM Ca^{2+} contained the following (in mM): 137 NaCl, 5.8 KCl, 0.04 $CaCl_2$ (buffered with N-(2-hydroxyethyl) ethylenediamine triacetic acid: HEDTA), 5.6 D-glucose, and 10 Na-HEPES, pH 7.5. To investigate the effects of DHS (Sigma), 100 mM stock solutions of DHS (molecular weight, 730.7) were prepared in the requisite intracellular or extracellular solution. During the recordings, all test solutions were present in the fluid jet and also superfused via a pipette positioned orthogonally to the axis of mechanical sensitivity of the hair bundle, so the flow did not directly stimulate the stereocilia. For every extracellular solution change (i.e., changing from the standard 1.3 mM Ca^{2+} to either 0.1 or 0.04 mM Ca^{2+}), the hair bundle was superfused with the new solution, and, before their stimulation, the fluid jet was filled with the same solution by suction through its tip using a negative gravity pressure system built in the fluid jet. Although this procedure allows to record the control MET current before the application of the different test solutions, the de-

gree of solution exchange in the fluid jet is unknown. To verify the reliability of our solution-exchange procedure in the fluid jet, we performed some experiments (21 of the 49 recordings used for Fig. 5) in which MET current was recorded with the fluid jet already prefilled with the different Ca^{2+} solutions. Because the two experimental procedures provided similar results, the data were pooled together in Figure 5.

To test whether MET current in mutant mice was regulated directly by the free Ca^{2+} inside the stereocilia, we investigated the influence of changing the intracellular Ca^{2+} buffering capacity. For these experiments, different concentrations (0.1–10 mM) of the fast Ca^{2+} buffer BAPTA (Invitrogen) was used instead of 1 mM EGTA (Fluka) in the above Cs-based intracellular solution. For the experiments investigating the effects of intracellular DHS, different concentration of the drug were added to the Cs-glutamate intracellular solution. When the concentration of BAPTA or DHS used was >1 mM, Cs-glutamate was adjusted to keep the osmolality constant.

Calcium selectivity. The calcium selectivity of the MET channel was calculated by measuring the reversal potential of calcium ($V_{rev}Ca^{2+}$) using a CsCl-based intracellular solution [in mM: 135 CsCl, 3 MgATP, 10 Tris phosphocreatine, 1 EGTA-CsOH, 10 HEPES-CsOH, pH 7.2 (osmolality, 293 mOsmol/kg)] and a high Ca^{2+} extracellular solution (in mM: 100 $CaCl_2$, 20 *N*-methylglucamine, 6 Tris, 10 D-glucose, adjusted to pH 7.4 with HCl), which was applied as described above. Reversal potentials were corrected for a liquid junction potential of −9 mV. The relative permeability, P_{Ca}/P_{Cs}, was calculated from the Goldman–Hodgkin–Katz equation: $P_{Ca}/P_{Cs} = \{a_1[Cs^+]/4a_2[Ca^{2+}]\} \times \{\exp(V_{rev}F/RT)\} \times \{1 + \exp(V_{rev}F/RT)\}$, where F/RT has its usual meaning with a value at room temperature of 25°C, $[Cs^+]$ and $[Ca^{2+}]$ are the concentrations of Cs^+ intracellularly (140 mM) and Ca^{2+} extracellularly (100 mM), and a_1 (0.711) and a_2 (0.519) are the published activity coefficients for Cs^+ (Partanen, 2010) and Ca^{2+} (Rard and Clegg, 1997), respectively.

Two-barrier one-binding-site model of DHS blockage of the MET channel. The voltage-dependent block of the transducer current by extracellular DHS was described quantitatively by a two-barrier one-binding-site model described in detail previously (Marcotti et al., 2005; Van Netten and Kros, 2007), according to the reaction scheme:

$$C + D_0 \underset{k_{-1}}{\overset{k_1}{\Leftrightarrow}} CD \underset{k_{-2}}{\overset{k_2}{\Leftrightarrow}} C + D_i,$$

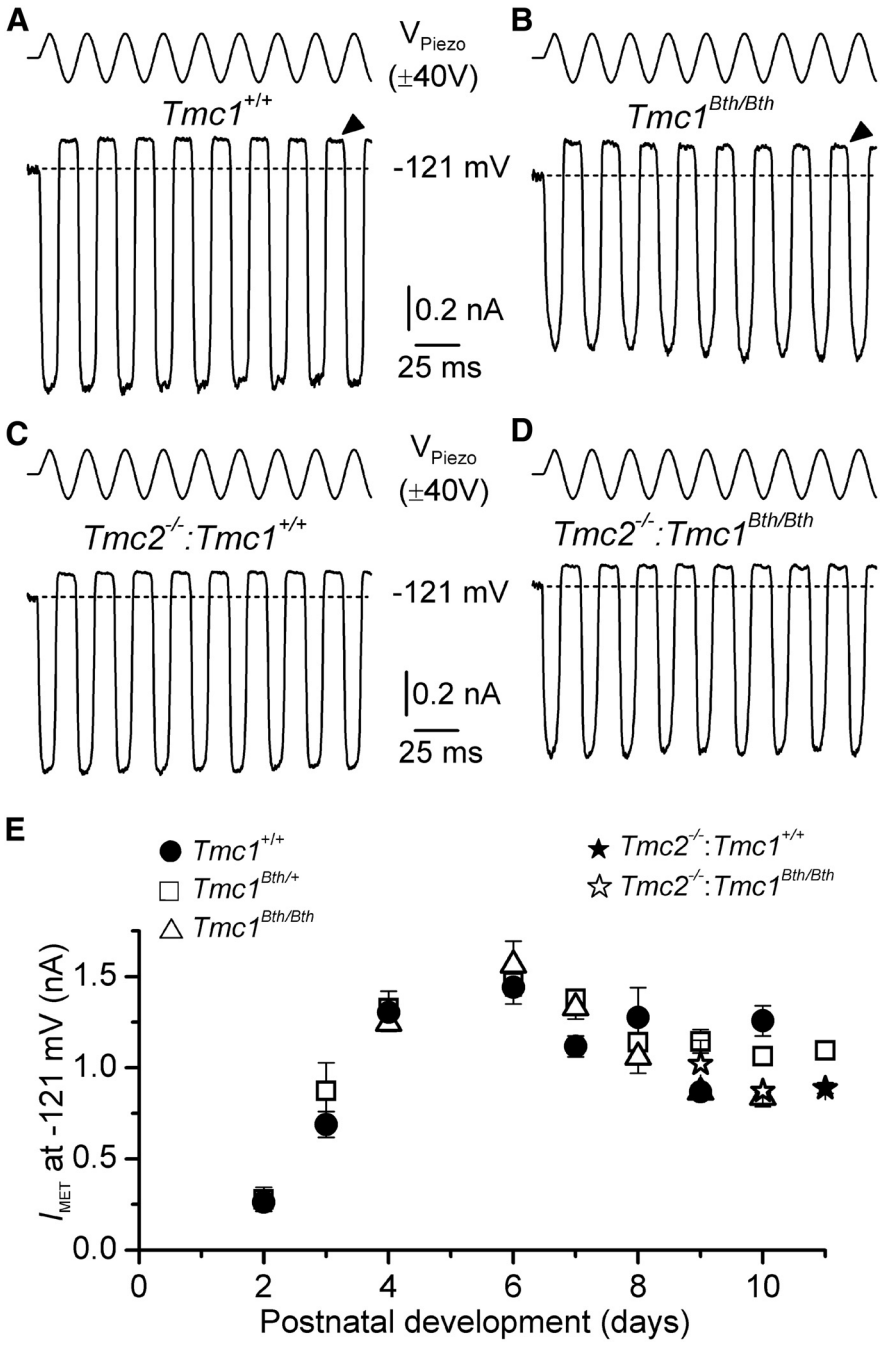

Figure 1. MET currents from *Tmc1*$^{Bth/Bth}$ and *Tmc2*$^{-/-}$:*Tmc1*$^{Bth/Bth}$ OHCs. ***A***, ***B***, Saturating MET currents in apical OHCs from P10 wild-type (*Tmc1*$^{+/+}$; ***A***) and homozygous mutant (*Tmc1*$^{Bth/Bth}$; ***B***) mice in response to a 50 Hz sinusoidal force stimulus to the hair bundles at a membrane potential of −121 mV. V_{Piezo} indicates the driver voltage to the fluid jet. Dashed lines indicate the holding current at −121 mV. The arrowheads indicate the closure of the MET channels, i.e., the disappearance of the resting MET current during inhibitory bundle displacements at −121 mV. ***C***, ***D***, MET currents in apical OHCs from the double-mutant *Tmc2*$^{-/-}$:*Tmc1*$^{+/+}$ (P11) and *Tmc2*$^{-/-}$:*Tmc1*$^{Bth/Bth}$ (P10) mice, respectively. ***E***, Absolute size of average saturating MET current at −121 mV recorded from OHCs of mice from the different genotypes (see labels above the panel) as a function of age. Number of OHCs from P2 to P11: *Tmc1*$^{+/+}$, 1, 3, 7, 6, 14, 3, 3, 3, 0; *Tmc1*$^{Bth/+}$, 3, 2, 10, 14, 10, 20, 6, 17, 1; and *Tmc1*$^{Bth/Bth}$, 0, 0, 5, 4, 8, 5, 5, 3, 0. Number of OHCs for *Tmc2*$^{-/-}$:*Tmc1*$^{+/+}$ was four (P11) and for *Tmc2*$^{-/-}$:*Tmc1*$^{Bth/Bth}$ was three (P9) and two (P10).

where C represents the unblocked MET channels, CD the blocked channels, and D_0 and D_i the extracellular and intracellular blockers. The forward (k_1, k_2) and backward (k_{-1}, k_{-2}) rate constants are voltage dependent, and the Hill coefficient $n_H = 1$. In brief, the voltage dependence of the block is expressed in four parameters: E_b, the free energy of the drug binding site at 0 membrane potential; δ_b, the fractional electrical distance of the site across the membrane from the extracellular side; $\Delta E = E_2 - E_1$, the difference between the intracellular and extracellular, respectively, free energy levels of the two barriers at 0 membrane potential; and $\Delta\delta = \delta_2 - \delta_1$, the fractional electrical distance between the barriers. Fits using this model and assuming a Hill coefficient of 1 (Marcotti et al., 2005) yield values for ΔE, E_b, $\Delta\delta$, and δ_b, where the binding

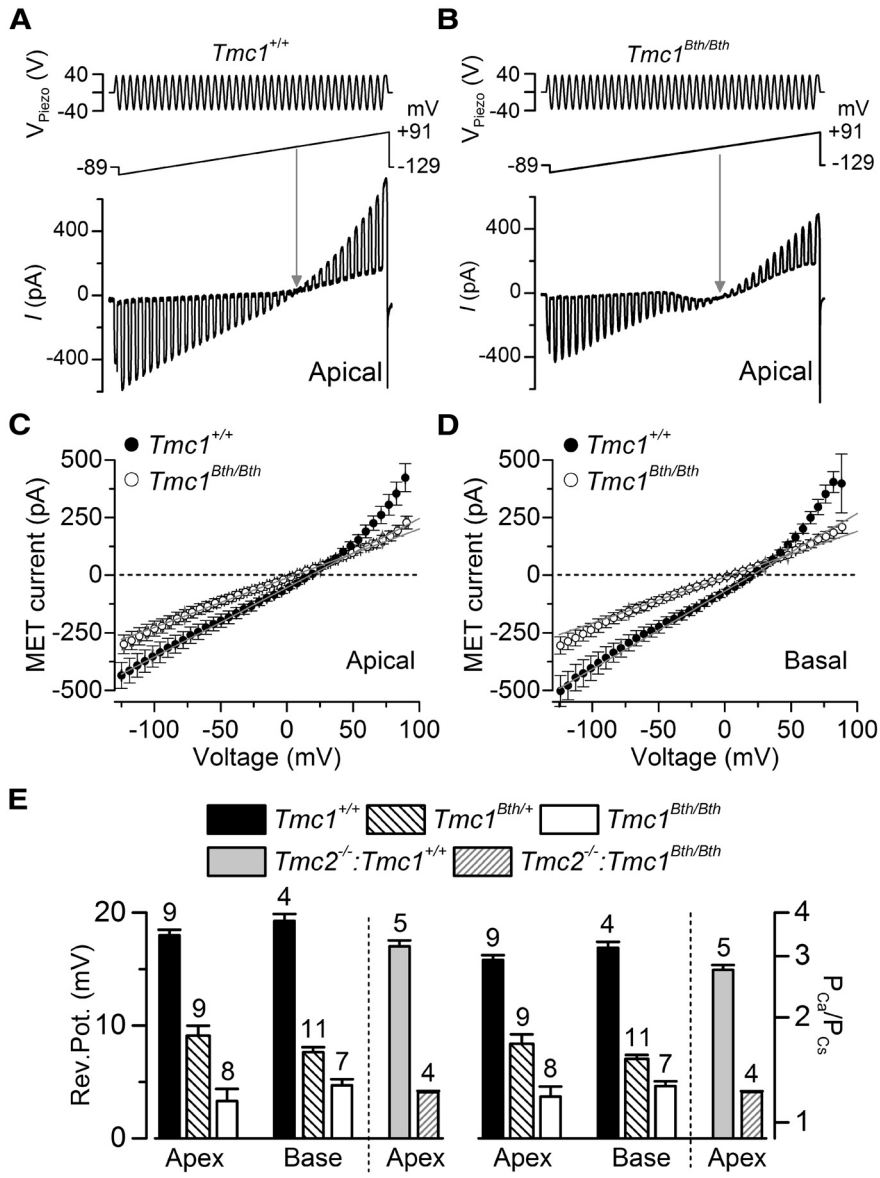

Figure 2. Calcium selectivity of the MET channel is reduced in $Tmc1^{Bth/Bth}$ mice. ***A***, ***B***, MET currents recorded from P6 apical OHCs from $Tmc1^{+/+}$ (***A***) and $Tmc1^{Bth/Bth}$ (***B***) mice in response to a 50 Hz sinusoidal force stimulus to the hair bundles superimposed to a voltage ramp (288 mV/s) from −129 to +91 mV nominal values (top panels). Arrows indicate the reversal potential of the MET current. ***C***, ***D***, Average MET current–voltage relationships recorded in apical (***C***) and basal (***D***) OHCs from $Tmc1^{+/+}$ and $Tmc1^{Bth/Bth}$ mice in the voltage region around reversal potential. Data are approximated with a linear regression line, with the following slope: apical, 3.0 pA/mV in $Tmc1^{+/+}$ and 2.1 pA/mV in $Tmc1^{Bth/Bth}$; and basal, 3.4 pA/mV in $Tmc1^{+/+}$ and 2.0 pA/mV in $Tmc1^{Bth/Bth}$. ***E***, Ca^{2+} reversal potential (left) and P_{Ca}/P_{Cs} (right). Number of OHCs tested is shown above the columns; apical OHCs, P6–P8; basal OHCs, P5–P7; apical OHCs from double mutant, P6–P7.

site is located at a relative electrical distance δ_b of 0.79 and $\Delta\delta$ is 0.91 (Marcotti et al., 2005). The forward rate constant k_1 was obtained from the slope of τ^{-1} versus $[D]_0$, allowing calculation of the absolute values of the energy barriers E_1 and E_2. This in turn enabled us to calculate k_2 and the entry rate of drug molecules into the OHCs.

Statistical analyses. Statistical comparisons of means were made by Student's two-tailed *t* test or for multiple comparisons by ANOVA (one-way ANOVA, followed by Tukey's test; two-way ANOVA, followed by Bonferroni's test). $p < 0.05$ was selected as the criterion for statistical significance. All values are quoted as mean ± SEM.

Results

MET currents in OHCs from *Beethoven* mutant mice

MET currents from OHCs of wild-type ($Tmc1^{+/+}$) and littermate mutant ($Tmc1^{Bth/+}$ and $Tmc1^{Bth/Bth}$) *Beethoven* mice were elicited by displacing their hair bundles with a piezoelectric fluid jet stimulator (Kros et al., 1992, Corns et al., 2014). Saturating bundle displacement in the excitatory direction (i.e., toward the taller stereocilia) elicited large inward MET currents in OHCs from $Tmc1^{+/+}$ and $Tmc1^{Bth/Bth}$ mice (Fig. 1*A*,*B*) and $Tmc1^{Bth/+}$ mice (data not shown). Inhibitory hair bundle stimulation (negative driver voltage) shut off the small fraction of current flowing at rest (Fig. 1*A*,*B*, arrowheads). Comparably large MET currents were also elicited in OHCs from double-mutant mice in which *Tmc2* was absent (Fig. 1*C*,*D*). The maximum amplitude of the MET current was similar at least up to P11 in all genotypes tested (Fig. 1*E*). These data demonstrate that the *Beethoven* mutation in *Tmc1* and loss of *Tmc2*, which is only expressed up to P8–P10 in apical OHCs (Kawashima et al., 2011), do not impair the size of the MET currents.

The ionic selectivity of the MET channel in *Beethoven* mice was determined by measuring its selectivity for Ca^{2+} over other cations. The hair bundles of OHCs from $Tmc1^{+/+}$ and $Tmc1^{Bth/Bth}$ mice were displaced using saturating stimuli superimposed on a voltage ramp (Fig. 2*A*,*B*) under conditions in which Ca^{2+} and Cs^{+} were the only permeant cations in the extracellular and intracellular solutions, respectively. The size of the MET currents in OHCs from both the apical and basal regions of the $Tmc1^{+/+}$ and $Tmc1^{Bth/Bth}$ cochleae is shown in Figure 2, *C* and *D*, respectively. The reversal potential of the MET current (Fig. 2*E*, left) was measured by fitting the *I–V* relationships from individual OHCs around the zero-current level with linear regression lines, which also allowed the calculation of the relative permeability, P_{Ca}/P_{Cs} (see equation in Materials and Methods; Fig. 2*E*, right). We found that the MET current reversal potential and relative Ca^{2+} permeability were similar between apical and basal OHCs, but both were reduced significantly ($p < 0.0001$) in $Tmc1^{Bth/Bth}$ OHCs compared with $Tmc1^{+/+}$ OHCs (Fig. 2*E*). The smaller Ca^{2+} permeability in $Tmc1^{Bth/Bth}$ was also associated with a reduced MET current slope conductance over the entire voltage range investigated (by ~30% for apical and by ~40% for basal OHCs; Fig. 2*C*,*D*, respectively). In $Tmc1^{Bth/+}$ heterozygotes, the Ca^{2+} selectivity was significantly different ($p < 0.0001$) from that of $Tmc1^{+/+}$ and $Tmc1^{Bth/Bth}$ in both apical and basal OHCs (one-way ANOVA; *post hoc* test was $p < 0.001$ between $Tmc1^{+/+}$ and $Tmc1^{Bth/+}$ in both cochlear regions, and $p < 0.01$ and $p < 0.05$ between $Tmc1^{Bth/Bth}$ and $Tmc1^{Bth/+}$ in apical and basal regions, respectively). Similar reductions in Ca^{2+} selectivity were also obtained

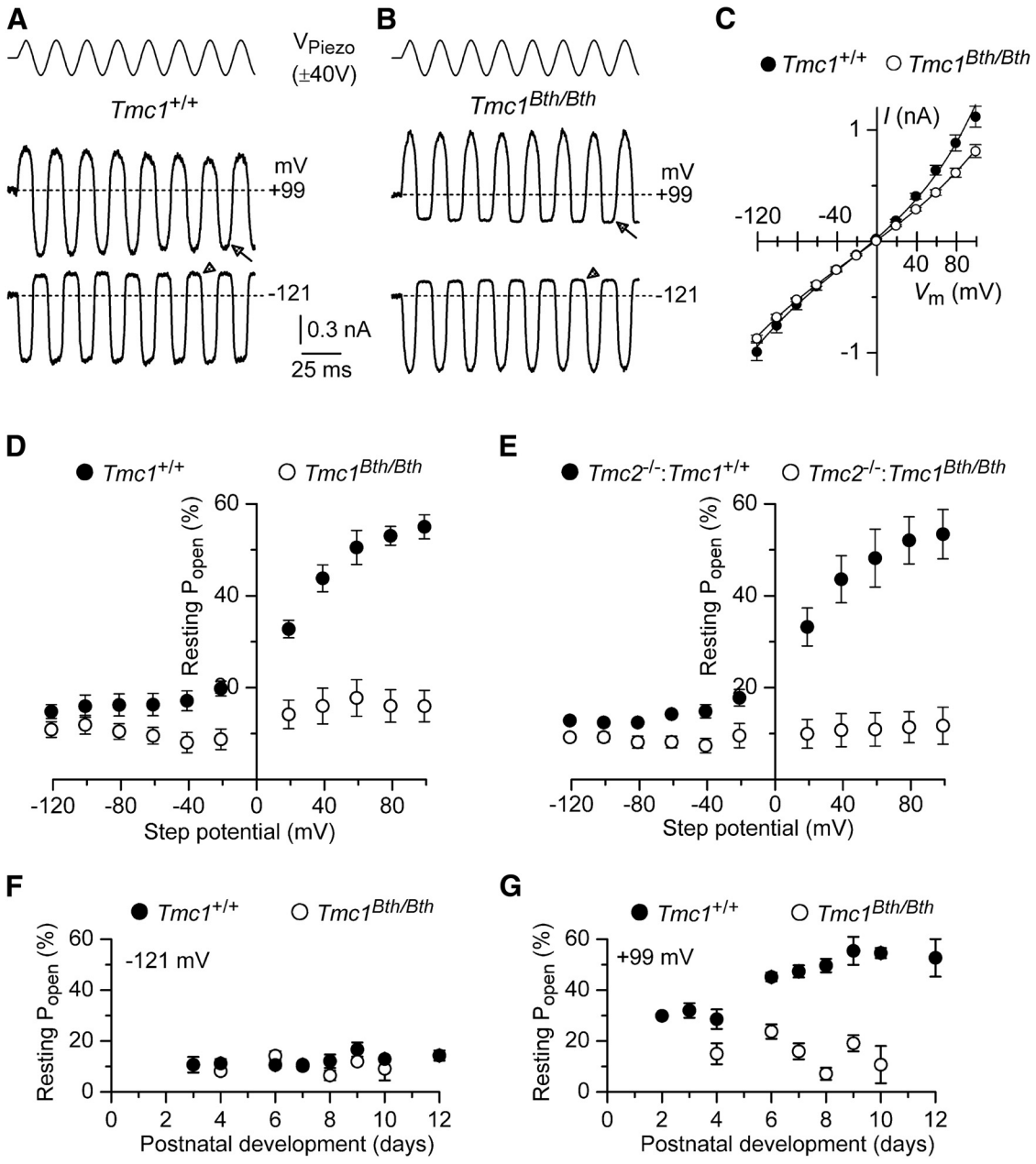

Figure 3. Fraction of MET channels open at rest is reduced in $Tmc1^{Bth/Bth}$ mice. ***A***, ***B***, Saturating MET currents in P9 apical OHCs from $Tmc1^{+/+}$ (***A***) and $Tmc1^{Bth/Bth}$ (***B***) mice in response to a 50 Hz sinusoidal force stimulus to the hair bundles at membrane potentials of −121 and +99 mV. The arrowheads and arrows indicate the closure of the transducer channels at −121 and + 99 mV, respectively. V_{Piezo} indicates the driver voltage to the fluid jet. ***C***, Peak-to-peak MET current–voltage curves obtained from five $Tmc1^{+/+}$ and seven $Tmc1^{Bth/Bth}$ OHCs (P9–P10) using 1.3 mM extracellular Ca^{2+}. ***D***, ***E***, Resting open probability (P_{open}) of the MET channel at increasing membrane potentials from −121 to +99 mV in $Tmc1^{+/+}$ ($n = 6$) and $Tmc1^{Bth/Bth}$ ($n = 8$) (***D***) and $Tmc2^{-/-}$:$Tmc1^{+/+}$ ($n = 4$) and $Tmc2^{-/-}$:$Tmc1^{Bth/Bth}$ ($n = 5$) (***E***) mice. ***F***, ***G***, Resting P_{open} of the MET channel at the holding potentials from −121 (***F***) and +99 mV (***G***) from P2 to P12 from $Tmc1^{+/+}$ and $Tmc1^{Bth/Bth}$ mice. Number of OHCs tested at −121 mV (***F***) and +99 mV (***G***) are as follows: $Tmc1^{+/+}$, 1, 3, 7, 6, 14, 3, 3, 3, 3; $Tmc1^{Bth/Bth}$, 0, 0, 5, 4, 8, 5, 5, 3, 0.

in double-mutant mice in which *Tmc2* was also absent (Fig. 2*E*, right). In both cases, the Ca^{2+} selectivity of the OHC MET channel was more than halved in $Tmc1^{Bth/Bth}$ relative to wild type; a comparable reduction in Ca^{2+} selectivity was reported in OHCs (Beurg et al., 2015) and inner hair cells (IHCs; Pan et al., 2013) of *Bth* mutants relative to wild type.

Effects of depolarization and extracellular Ca^{2+} on the MET current of OHCs from *Beethoven* mice

Calcium has been reported to modulate the fraction of the MET current activated in the absence of bundle stimulation. Although increasing Ca^{2+} influx through the MET channels promotes closing of some of the channels, measures to reduce Ca^{2+} influx into the channel, by either lowering its extracellular concentration or depolarizing the cell to near the Ca^{2+} equilibrium potential, have been reported to increase channel open probability (Assad et al., 1989; Crawford et al., 1991; Ricci et al., 1998; Corns et al., 2014). Large MET currents could be recorded from OHCs of $Tmc1^{+/+}$ (Fig. 3*A*) and $Tmc1^{Bth/Bth}$ (Fig. 3*B*) mice at both negative (−121 mV) and positive (+99 mV) membrane potentials. OHC membrane depolarization caused the MET current to decrease in size at first and then reverse near 0 mV to become

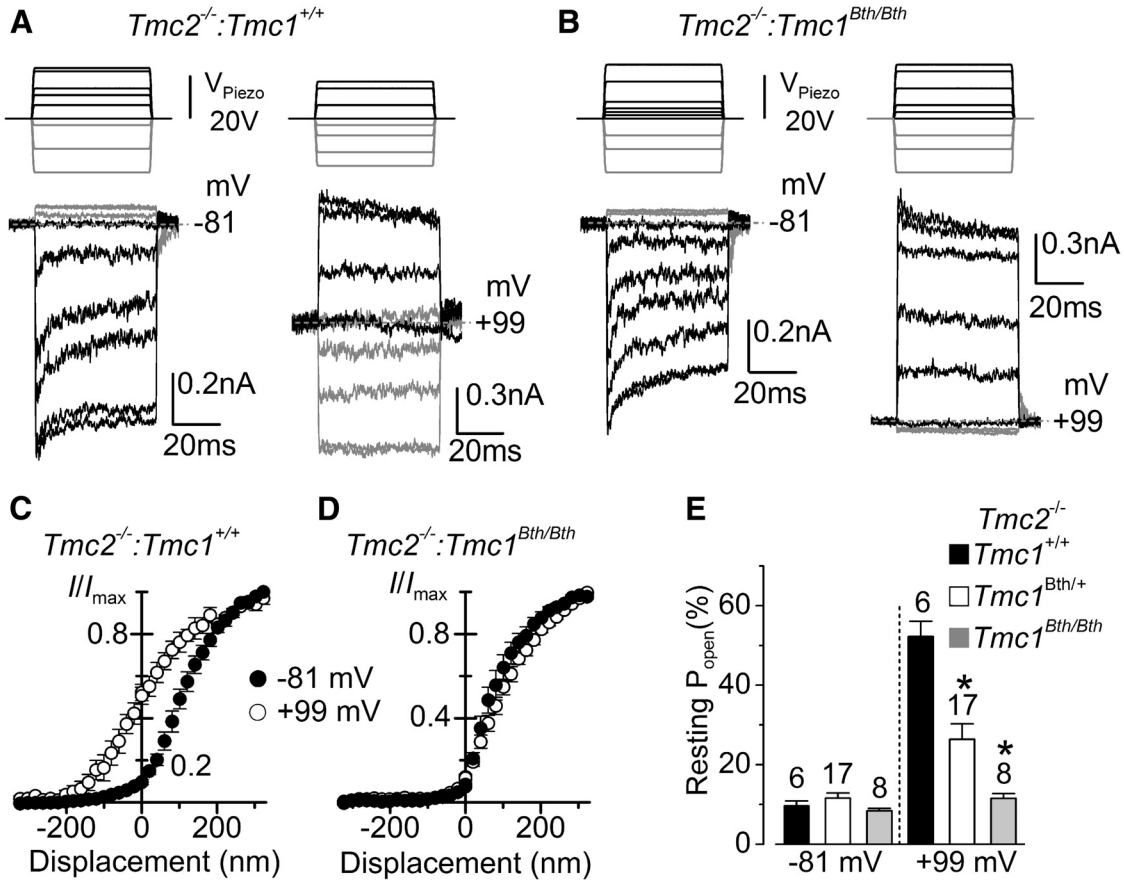

Figure 4. Depolarization-induced shift in OHC current-displacement relation is reduced in *Tmc1* mutants. ***A***, ***B***, MET currents recorded at −81 mV (left panels) and +99 mV (right panels) from *Tmc2*$^{-/-}$:*Tmc1*$^{+/+}$ (***A***; P8) and *Tmc2*$^{-/-}$:*Tmc1*$^{Bth/Bth}$ (***B***; P7) apical OHCs elicited using force-step stimuli (top panels). At −81 mV, positive driver voltages of 50 ms duration (excitatory direction) elicited inward MET currents that declined or adapted over time. A small transducer current was present at rest and inhibitory bundle displacements turned this off (gray traces). At +99 mV (right), adaptation was absent and the resting MET current open at rest was increased only in *Tmc2*$^{-/-}$:*Tmc1*$^{+/+}$ OHCs. The MET currents recorded at −81 and +99 mV are from the same OHCs. ***C***, ***D***, Normalized peak MET current recorded from *Tmc2*$^{-/-}$:*Tmc1*$^{+/+}$ (***C***; P6–P9, $n = 5$) and *Tmc2*$^{-/-}$:*Tmc1*$^{Bth/Bth}$ (***D***; P6–P7, $n = 8$) OHCs at the holding potential of −81 mV and during a step to +99 mV as a function of bundle displacement. Note the leftward shift in the relation at +99 mV for the MET current recorded from *Tmc2*$^{-/-}$:*Tmc1*$^{+/+}$ mice only. The average saturating MET current in OHCs was 869 ± 103 pA (*Tmc2*$^{-/-}$:*Tmc1*$^{+/+}$) and 855 ± 47 pA (*Tmc2*$^{-/-}$:*Tmc1*$^{Bth/Bth}$) at −81 mV and 1450 ± 187 pA (*Tmc2*$^{-/-}$:*Tmc1*$^{+/+}$) and 1125 ± 80 pA (*Tmc2*$^{-/-}$:*Tmc1*$^{Bth/Bth}$) at +99 mV. ***E***, Resting P_{open} at −81 and +99 mV in the three different genotypes.

outward at positive potentials (Fig. 3*C*), in accordance with the nonselective permeability of MET channels to cations (Ohmori, 1985). The fraction of the MET current open at rest is usually larger at positive compared with negative membrane potentials (Fig. 3*A*,*D*: *Tmc1*$^{+/+}$). We found that *Tmc1*$^{Bth/Bth}$ OHCs did not show any increase in the resting open probability (P_{open}) of the MET channel with membrane depolarization (Fig. 3*B*,*D*). Similar findings were also seen in the double-mutant mice in which *Tmc2* was absent (Fig. 3*E*). At −121 mV, the resting P_{open} was relatively constant up to P12 in both *Tmc1*$^{+/+}$ and *Tmc1*$^{Bth/Bth}$ OHCs (Fig. 3*F*). At positive membrane potentials (+99 mV), although the resting P_{open} in *Tmc1*$^{+/+}$ OHCs gradually increased with development ($p < 0.0001$, one-way ANOVA), that of *Tmc1*$^{Bth/Bth}$ OHCs was found to be significantly smaller ($p < 0.0005$, two-way ANOVA) than that of *Tmc1*$^{+/+}$ and relatively unchanged during the same time window (Fig. 3*G*). These findings suggest that the mutation in *Beethoven* mice strongly reduces the normal effect of depolarization on the resting MET current but independent from the presence or absence of Tmc2.

We then stimulated the hair bundle with 50 ms force steps to further investigate the dynamic adaptation properties of the MET current (Fig. 4). Upon deflecting the bundles in the excitatory direction, at −81 mV in the presence of 1.3 mM extracellular Ca^{2+}, adaptation or time-dependent decline of the MET current occurred for small bundle displacements in OHCs from both *Tmc2*$^{-/-}$:*Tmc1*$^{+/+}$ and *Tmc2*$^{-/-}$:*Tmc1*$^{Bth/Bth}$ mice (Fig. 4*A*,*B*, left panels, respectively). Inhibitory hair bundle deflection shut off the small fraction of the current flowing at rest. All these manifestations of MET current adaptation were lost on stepping the membrane potential to +99 mV (Fig. 4*A*,*B*, right panels), a condition that prevents or strongly reduces Ca^{2+} entry via the MET channels. Stepping the membrane potential from −81 to +99 mV increased the resting P_{open} of the MET channel in OHCs from *Tmc2*$^{-/-}$:*Tmc1*$^{+/+}$ (Fig. 4*A*,*C*) but not from *Tmc2*$^{-/-}$:*Tmc1*$^{Bth/Bth}$ mice (Fig. 4*B*,*D*), which is indicated by the lack of a leftward shift in the relationship between the normalized MET current and bundle displacement in the *Beethoven* mutant (Fig. 4*D*). The resting P_{open} at −81 mV was similar between *Tmc1*$^{+/+}$, *Tmc1*$^{Bth/+}$, and *Tmc1*$^{Bth/Bth}$ (all were knock-outs for *Tmc2*; Fig. 4*E*, left). However, at +99 mV, the resting P_{open} in *Tmc2*$^{-/-}$:*Tmc1*$^{+/+}$ was significantly larger compared with both *Tmc2*$^{-/-}$:*Tmc1*$^{Bth/+}$ and *Tmc2*$^{-/-}$:*Tmc1*$^{Bth/Bth}$ ($p < 0.001$, one-way ANOVA *post hoc* tests).

We further tested the effects of Ca^{2+} on the MET current of *Beethoven* mutants by comparing experiments in 1.3 mM Ca^{2+} and low extracellular Ca^{2+} (0.04 and 0.1 mM). These low Ca^{2+}

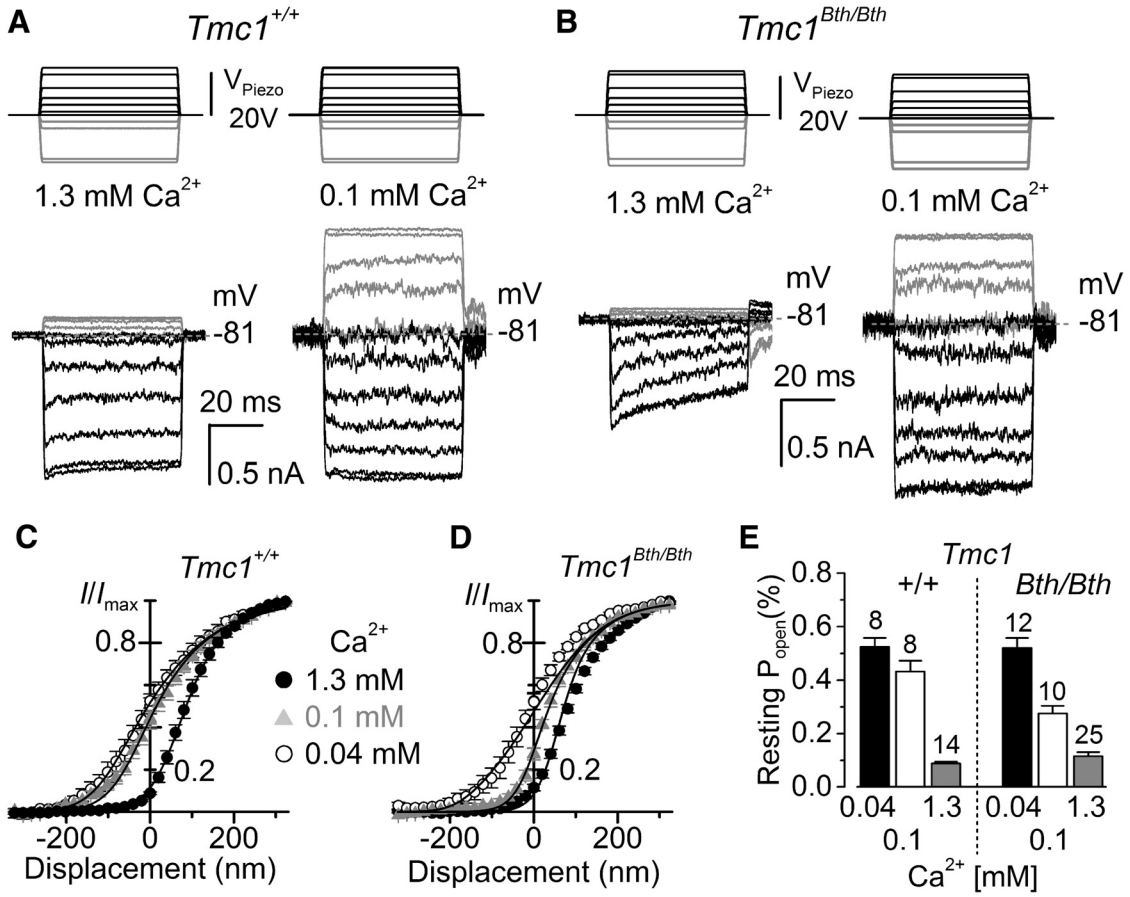

Figure 5. The shift of the MET current-displacement relation of *Tmc1* mutant OHCs is more responsive to increasing extracellular Ca^{2+}. ***A***, ***B***, MET currents recorded from *Tmc1*$^{+/+}$ (***A***) and *Tmc1*$^{Bth/Bth}$ (***B***) P7 apical OHCs in response to step driver-voltages to the fluid jet (top). Both OHCs were recorded at the holding potential of −81 mV in the presence of 1.3 mM Ca^{2+} and 0.1 mM Ca^{2+} in the extracellular solution. ***C***, ***D***, Normalized MET currents recorded from P6–P7 apical OHCs from *Tmc1*$^{+/+}$ (***C***) and *Tmc1*$^{Bth/Bth}$ (***D***) mice in the presence of 1.3 mM and low extracellular Ca^{2+} (0.1 and 0.04 mM). The MET currents in the presence of different extracellular Ca^{2+} concentrations were obtained by stimulating their hair bundle in one of the two following conditions: 21 OHCs were recorded with the fluid jet already prefilled with 1.3, 0.1, or 0.04 mM Ca^{2+}; 28 OHCs were recorded in both 1.3 mM Ca^{2+} and either 0.1 or 0.04 mM Ca^{2+} (see Materials and Methods). The data were fitted using a second-order Boltzmann function: $I/I_{max} = 1/(1 + \exp(a_2(x_2 - x)) \times (1 + \exp(a_1(x_{1\_} x))))$. The saturating MET current (I_{max}) in *Tmc1*$^{+/+}$ was 1096 ± 67 pA ($n = 14$) in 1.3 mM Ca^{2+}, 1376 ± 200 pA ($n = 8$) in 0.1 mM Ca^{2+}, and 1792 ± 179 pA ($n = 8$); in 0.04 mM Ca^{2+}, in *Tmc1*$^{Bth/Bth}$ I_{max} was 918 ± 22 pA ($n = 25$) in 1.3 mM Ca^{2+}, 1801 ± 76 pA ($n = 10$) in 0.1 mM Ca^{2+}, and 1749 ± 84 pA, ($n = 12$) in 0.04 mM Ca^{2+}. Apart from x_1, all other values were identical among the fits (*Tmc1*$^{+/+}$: $a_1 = 0.018\ nm^{-1}$, $a_2 = 0.010\ nm^{-1}$, $x_2 = -26$ nm; *Tmc1*$^{Bth/Bth}$: $a_1 = 0.027\ nm^{-1}$, $a_2 = 0.012\ nm^{-1}$, $x_2 = 8$ nm). For x_1, the values were as follows: in *Tmc1*$^{+/+}$, 122 nm in 1.3 mM Ca^{2+}, −26 nm in 0.1 mM Ca^{2+}, −90 nm in 0.04 mM Ca^{2+}; and in *Tmc1*$^{Bth/Bth}$, 80 nm in 1.3 mM Ca^{2+}, 8 nm in 0.1 mM Ca^{2+}, −177 nm in 0.04 mM Ca^{2+}. Note the larger shift in x_1 in *Bth* mutants compared with that of wild type on increasing Ca^{2+} from 0.04 to 0.1 mM (*Tmc1*$^{Bth/Bth}$, 185 nm; *Tmc1*$^{+/+}$, 64 nm), although it was reduced when going from 0.1 to 1.3 mM (*Tmc1*$^{Bth/Bth}$, 72 nm; *Tmc1*$^{+/+}$, 148 nm). ***E***, Resting P_{open} at −81 mV for the different Ca^{2+} concentrations and genotypes.

concentrations were selected because, although the bundles of adult mouse hair cells are surrounded by endolymph containing 0.02–0.04 mM Ca^{2+} (Bosher and Warren, 1978; Salt et al., 1989), immature cells are exposed to an estimated *in vivo* endolymphatic Ca^{2+} concentration in the low millimolar range (≤0.3 mM; Johnson et al., 2012). In OHCs from both *Tmc1*$^{+/+}$ and *Tmc1*$^{Bth/Bth}$ mice, reducing the extracellular Ca^{2+} concentration from 1.3 to 0.1 mM (Fig. 5*A*,*B*, respectively) or 0.04 mM (data not shown) at −81 mV increased the MET channel resting P_{open} as reported previously (Johnson et al., 2011; Corns et al., 2014). However, the overall dependence of P_{open} on extracellular Ca^{2+} was found to be significantly different between the two genotypes ($p < 0.01$, two-way ANOVA; Fig. 5*C–E*), with the *post hoc* test analysis revealing a significant difference for only 0.1 mM Ca^{2+} between *Tmc1*$^{+/+}$ and *Tmc1*$^{Bth/Bth}$ ($p < 0.001$). Furthermore, although in *Tmc1*$^{+/+}$ the P_{open} was similar between 0.1 and 0.04 mM Ca^{2+}, in *Tmc1*$^{Bth/Bth}$ it was significantly reduced in the former ($p < 0.001$, one-way ANOVA). This points to an increased sensitivity of the open probability of the resting MET current to extracellular Ca^{2+} in *Tmc1*$^{Bth/Bth}$. These findings differ from a recent report showing that the P_{open} of the MET current in *Beethoven* OHCs was only slightly affected when reducing the extracellular Ca^{2+} from 1.3 to 0.04 mM (Beurg et al., 2015), but within the range we have reported for the 0.1 mM Ca^{2+} solution (Fig. 5*C–E*). This discrepancy in Ca^{2+} sensitivity may have been attributable to incomplete exchange of the solution in the fluid jet used to stimulate the hair bundle when changing the different Ca^{2+} concentrations (Beurg et al., 2015).

Lowering the extracellular Ca^{2+} concentration also had the effect of increasing the size of the MET current (Fig. 5*A*,*B*), which stems from relief of the block by Ca^{2+} in the permeation pathway of the channel (Ricci and Fettiplace, 1998; Marcotti et al., 2005). For the experiments in which the MET current was recorded in 1.3 mM and either 0.1 or 0.04 mM extracellular Ca^{2+} from the same OHCs (see Materials and Methods), we found that the MET current size ratio (1.3/0.1 mM Ca^{2+} or 1.3/0.04 mM Ca^{2+}) recorded at −81 mV was significantly smaller in *Tmc1*$^{Bth/Bth}$ (1.3/0.1 mM Ca^{2+} = 0.5280 ± 0.0199, $n = 9$, $p < 0.002$; 1.3/0.04 mM

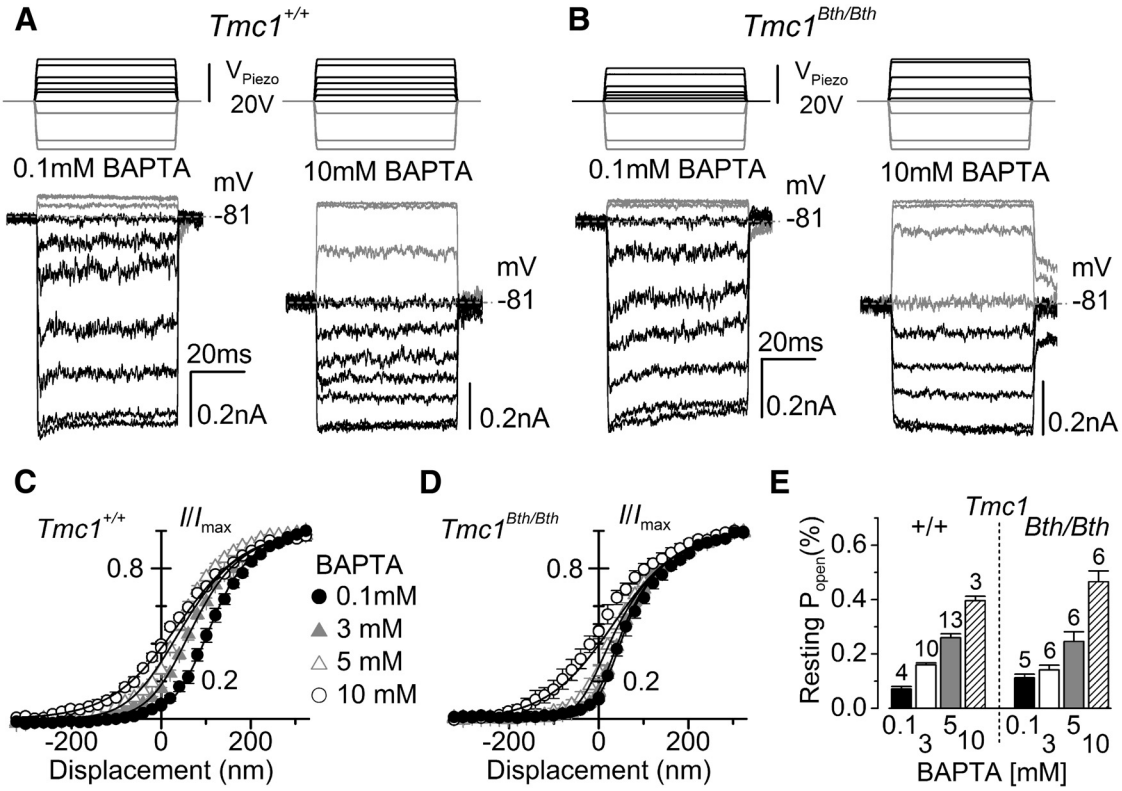

Figure 6. Increasing intracellular BAPTA increased resting MET currents in *Beethoven* mutant OHCs less than in control OHCs. ***A***, ***B***, MET currents recorded from apical OHCs of *Tmc1* $^{+/+}$ (***A***; P6) and *Tmc1*$^{Bth/Bth}$ (***B***; P7) in response to step driver voltages to the fluid jet (top) and in the presence of either 0.1 or 10 mM BAPTA in the intracellular solution. All experiments were performed at the holding potential of −81 mV. ***C***, ***D***, Average normalized peak MET current at −81 mV as a function of hair bundle displacement in the presence of different BAPTA concentrations from *Tmc1* $^{+/+}$ (P6–P8) and *Tmc1*$^{Bth/Bth}$ (P7–P8) OHCs. The data were fitted using the equation in Figure 5. I_{max} values were as follows: in *Tmc1* $^{+/+}$, 0.1 mM, −964 ± 42 pA ($n = 4$); 3 mM, −811 ± 39 pA ($n = 10$); 5 mM, −974 ± 41 pA ($n = 13$); 10 mM, −958 ± 108 pA ($n = 3$); in *Tmc1*$^{Bth/Bth}$, 0.1 mM, −716 ± 64 pA ($n = 5$); 3 mM, −929 ± 90 pA ($n = 6$); 5 mM, −880 ± 64 pA ($n = 6$); 10 mM, −717 ± 38 pA ($n = 6$). Apart from x_1, all other values were identical among the fits (*Tmc1* $^{+/+}$: $a_1 = 0.015$ nm $^{-1}$, $a_2 = 0.013$ nm $^{-1}$, $x_2 = 38$ nm; *Tmc1*$^{Bth/Bth}$: $a_1 = 0.030$ nm $^{-1}$, $a_2 = 0.014$ nm $^{-1}$, $x_2 = 32$ nm). For x_1, the values were as follows: *Tmc1* $^{+/+}$, 146 nm in 0.1 mM, 38 nm in 3 mM, −64 nm in 5 mM, −426 nm in 10 mM; in *Tmc1*$^{Bth/Bth}$, 44 nm in 0.1 mM, 32 nm in 3 mM, −11 nm in 5 mM, −297 nm in 10 mM. ***E***, Resting P_{open} in *Tmc1* $^{+/+}$ and *Tmc1*$^{Bth/Bth}$ OHCs at −81 mV and at different BAPTA concentrations.

Ca^{2+} = 0.5153 ± 0.0178, $n = 9$, $p < 0.02$) than in *Tmc1* $^{+/+}$ OHCs (1.3/0.1 mM Ca^{2+} = 0.6976 ± 0.0422, $n = 4$; 1.3/0.04 mM Ca^{2+} = 0.6106 ± 0.0285, $n = 6$). A smaller ratio in the mutants implies a stronger Ca^{2+} block of the MET current in the presence of 1.3 mM Ca^{2+} in *Tmc1*$^{Bth/Bth}$ OHCs, which is in agreement with the reduced Ca^{2+} permeability and conductance observed in these cells, and all these findings indicate that the *Beethoven* point mutation directly affects the MET channel Ca^{2+} binding site located within the channel. A similar stronger Ca^{2+} block of the MET current has also been reported in *Beethoven* mouse IHCs (Pan et al., 2013).

Intracellular calcium modulation of MET currents in OHCs of *Beethoven* mice

We tested whether MET currents of Tmc1$^{Bth/Bth}$ OHCs were directly regulated by free Ca^{2+} inside the stereocilia by changing the intracellular Ca^{2+} buffering capacity. We recorded MET currents at −81 mV in the presence of different concentrations of the fast Ca^{2+} buffer BAPTA (Fig. 6). In the presence of 0.1 mM BAPTA, nonsaturating bundle displacements caused the MET current to adapt in both genotypes (Fig. 6*A*,*B*, left panels), exactly as seen when 1 mM EGTA was used in the intracellular solution (Fig. 4). In the presence of 10 mM intracellular BAPTA, the time-dependent MET current decline was abolished and the resting P_{open} increased to near 50% of the maximal MET current in OHCs from both *Tmc1* $^{+/+}$ (Fig. 6*A*, right) and *Tmc1*$^{Bth/Bth}$ (Fig. 6*B*, right) mice. The relation between the MET current and bundle displacement (Fig. 6*C*,*D*) shows that increasing the intracellular BAPTA concentration from 0.1 to 10 mM significantly increased ($p < 0.0001$) the resting P_{open} of the MET current in both *Tmc1* $^{+/+}$ (0.1 mM, 8.0 ± 1.6%, $n = 4$; 10 mM, 39.6 ± 2.7%, $n = 5$) and *Tmc1*$^{Bth/Bth}$ (0.1 mM, 10.4 ± 2.2%, $n = 3$; 10 mM, 46.5 ± 9.9%, $n = 6$). No significant differences were seen between the two genotypes for both BAPTA concentrations. However, 3 and 5 mM BAPTA were less effective in shifting the MET current-bundle displacement curves in *Tmc1*$^{Bth/Bth}$ than in *Tmc1* $^{+/+}$ OHCs (Fig. 6*C*,*D*). In *Tmc1* $^{+/+}$, increasing the BAPTA concentration from 0.1 mM to either 3 or 5 mM produced a highly significant increase in P_{open} (*post hoc* test from one-way ANOVA, $p < 0.01$ and $p < 0.001$, respectively; Fig. 6*E*); in *Tmc1*$^{Bth/Bth}$, the same comparison produced no or a much reduced increase in P_{open} (n.s. and $p < 0.05$, respectively; Fig. 6*E*).

Effects of DHS on the MET current in *Beethoven* mice

DHS is known to block the MET channel in hair cells of both nonmammals (Kroese et al., 1989; Ohmori, 1985; Ricci, 2002) and mammals, in which it has been shown to enter the cell by traversing the channel, i.e., it is a permeant blocker (Marcotti et al., 2005). The dependence of the DHS-induced channel block on extracellular Ca^{2+} and membrane potential (Kroese et al., 1989; Ricci, 2002; Marcotti et al., 2005) has led to the suggestion that the drug-binding site is within the permeation pathway of the

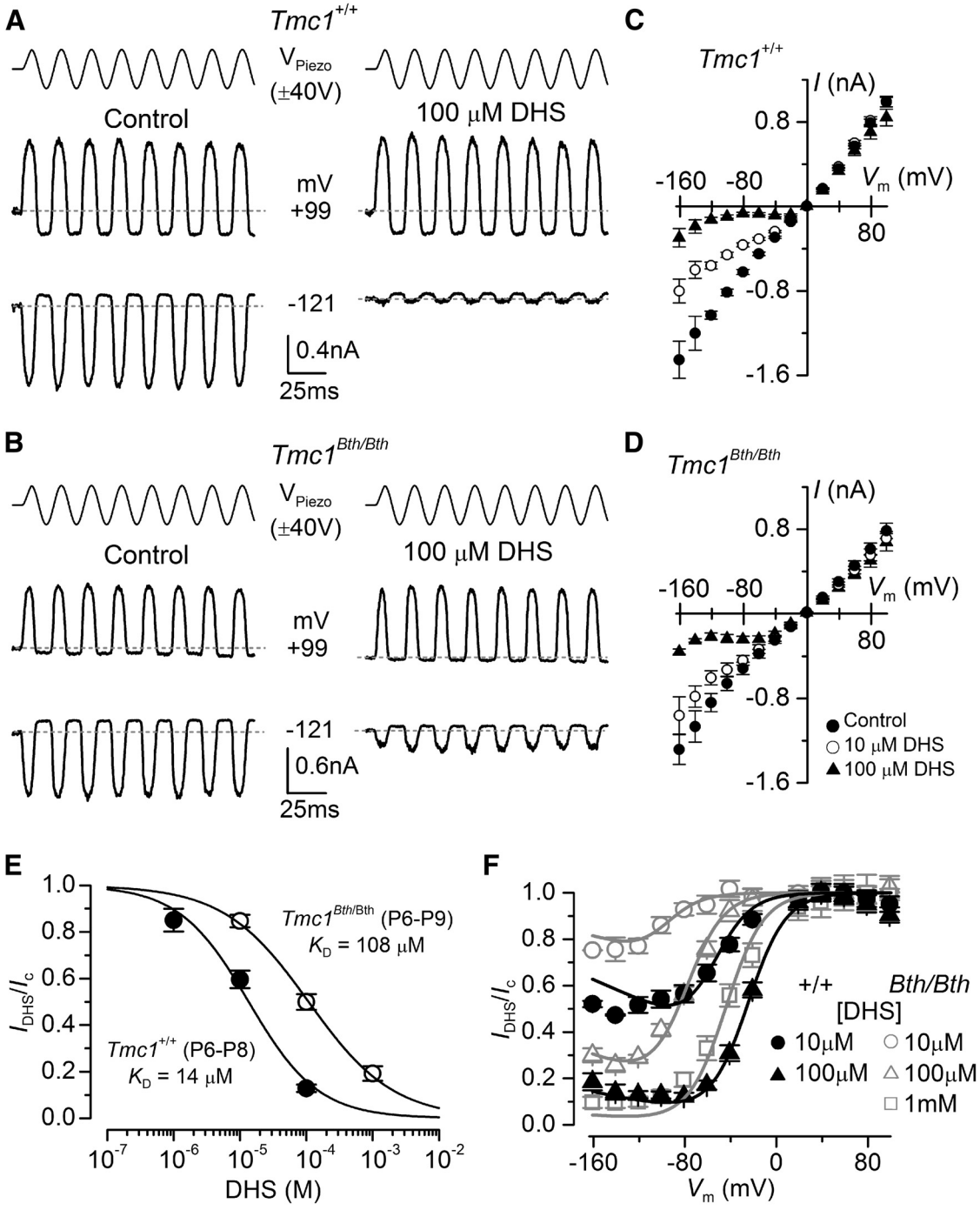

Figure 7. The MET channel of OHCs of *Beethoven* mice has a reduced affinity to DHS. ***A***, ***B***, Block of saturating MET current by extracellular DHS in apical OHCs of *Tmc1* $^{+/+}$ (***A***) and *Tmc1*$^{Bth/Bth}$ (***B***) mice in response to sinusoidal stimuli to the hair bundles (top) and at membrane potentials of −121 and +99 mV. Recordings were performed in the presence of 100 μM extracellular DHS. ***C***, ***D***, Average normalized MET current–voltage curves recorded from OHCs of P7–P8 *Tmc1* $^{+/+}$ (***C***) and P6–P9 *Tmc1*$^{Bth/Bth}$ (***D***) for some of the DHS concentrations tested. Numbers of OHCs recorded under the different conditions were as follows: *Tmc1* $^{+/+}$ control conditions ($n = 16$), 10 μM DHS ($n = 15$), 100 μM DHS ($n = 14$); *Tmc1*$^{Bth/Bth}$ control conditions ($n = 7$), 10 μM DHS ($n = 7$), 100 μM DHS ($n = 6$). ***E***, Dose–response curves for the block of the MET current by extracellular DHS at −81 mV in OHCs from *Tmc1* $^{+/+}$ (filled symbol) and *Tmc1*$^{Bth/Bth}$ (open symbol). Continuous lines are fits through the data using a Hill equation. *Tmc1* $^{+/+}$ OHCs (P6–P8) half-blocking concentration of K_D of 14 ± 4 μM and a Hill coefficient n_H of 0.82 ± 0.18 (number of OHCs from left to right: 3, 15, 14); *Tmc1*$^{Bth/Bth}$ OHCs (P6–P8) half-blocking concentration of K_D of 108 ± 11 μM and a Hill coefficient n_H of 0.68 ± 0.48 (number of OHCs from left to right: 7, 6, 6). ***F***, Voltage-dependent block of the transducer current by DHS. MET currents recorded in the presence of different concentrations of DHS were plotted as a fraction of the current in the control solution. Number of cells is as in ***E***. Continuous lines are fits according to the two-barrier one-binding-site model (see Materials and Methods). The fitted parameters are as follows: $\Delta\delta = \delta_2 - \delta_1$: 0.91, and δ_b: 0.79 for all conditions tested; ΔE was 4.83 *kT* in *Tmc1* $^{+/+}$ and 7.32 *kT* in *Tmc1*$^{Bth/Bth}$; E_b was −7.65 *kT* in *Tmc1* $^{+/+}$ and −4.21 *kT* in *Tmc1*$^{Bth/Bth}$.

channel, and this binding site is accessible from both intracellular and extracellular sides of the plasma membrane (Marcotti et al., 2005; van Netten and Kros, 2007). MET currents were mainly recorded by stepping the membrane between −121 and +99 mV in 20 mV increments, although in some experiments, we extended the voltage range to between −161 and +159 mV. Using 50 Hz sinusoidal stimulation, we recorded the MET current from OHCs of both *Tmc1* $^{+/+}$ and *Tmc1*$^{Bth/Bth}$ in the presence of dif-

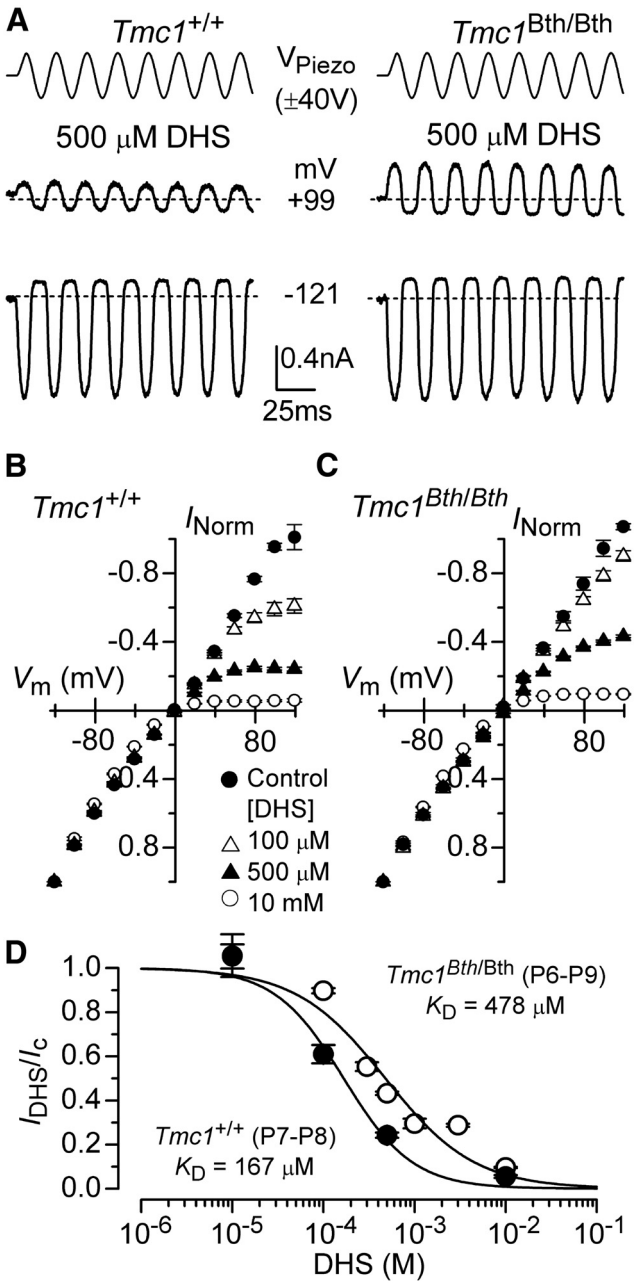

Figure 8. Reduced block by intracellular DHS in OHCs of *Beethoven* mice. ***A***, Block of MET current by intracellular DHS in apical P7 OHCs of $Tmc1^{+/+}$ (left) and $Tmc1^{Bth/Bth}$ (right) mice at membrane potentials of −121 and +99 mV in the presence of 500 μM DHS. Experimental protocol as described in Figure 7. ***B***, ***C***, Average normalized MET current–voltage curves from OHCs of P7–P8 $Tmc1^{+/+}$ (***B***) and P6–P9 $Tmc1^{Bth/Bth}$ (***C***) for some of DHS concentrations tested. Note that intracellular DHS blocks the MET current at depolarized potentials in OHCs from both genotypes. Numbers of OHCs recorded under the different conditions were as follows: $Tmc1^{+/+}$ control conditions ($n = 16$), 100 μM DHS ($n = 5$), 500 μM DHS ($n = 8$), and 10 mM DHS ($n = 6$); $Tmc1^{Bth/Bth}$ control conditions ($n = 7$), 100 μM DHS ($n = 6$), 500 μM DHS ($n = 13$), and 10 mM DHS ($n = 6$). ***D***, Dose–response curves for the block of the MET current by intracellular DHS at +119 mV in OHCs from $Tmc1^{+/+}$ (filled symbols) and $Tmc1^{Bth/Bth}$ (open symbols). Continuous lines are fits through the data using a Hill equation. $Tmc1^{+/+}$ OHCs (P7–P8) half-blocking concentration of K_D of 167 ± 40 μM and a Hill coefficient n_H of 1.1 ± 0.3 (number of OHCs from left to right: 5, 5, 8, 6); $Tmc1^{Bth/Bth}$ OHCs (P6–P9) half-blocking concentration of K_D of 479 ± 104 μM and a Hill coefficient *n*H of 0.9 ± 0.2 (number of OHCs from left to right: 3, 4, 5, 13, 5, 4, 6).

ferent concentrations of extracellular (Fig. 7) and intracellular (Fig. 8) DHS. As described previously (Marcotti et al., 2005), extracellular DHS caused a voltage-dependent block of the MET current, pronounced at negative membrane potentials and relieved at positive potentials in both genotypes (Fig. 7*A*,*B*). The normalized current–voltage curves for the peak-to-peak MET current with and without extracellular DHS are shown in Figure 7, *C* ($Tmc1^{+/+}$) and *D* ($Tmc1^{Bth/Bth}$). The concentration for half block (K_D) of the MET current at −81 mV in $Tmc1^{Bth/Bth}$ (108 μM) was nearly eight times higher than that measured in $Tmc1^{+/+}$ (14 μM; Fig. 7*E*). The voltage dependence of the block of the MET channel by DHS was investigated further by plotting the MET current in OHCs in the presence of the drug as a fraction of the control current (I_{DHS}/I_c; Fig. 7*F*). The block of the MET current by DHS is partially relieved for values negative to approximately −80 mV in both genotypes. This behavior is consistent with DHS being pushed from its binding site and forced through the channel pore into the cytoplasm when sufficient electrical driving force is applied (Marcotti et al., 2005), indicating that DHS can still permeate the MET channel in *Bth* mutant mice. The fits through the data are according to the two-barrier one-binding-site model (Marcotti et al., 2005). Intracellular application of DHS inhibited the MET current at positive potentials in a similar dose-dependent manner in both $Tmc1^{+/+}$ and $Tmc1^{Bth/Bth}$ OHCs (Fig. 8*A*–*C*) but, as described previously (Marcotti et al., 2005), with a reduced potency compared with extracellular DHS. In $Tmc1^{Bth/Bth}$ OHCs, the K_D for intracellular DHS block was 478 μM, which was nearly three times higher than that measured in for $Tmc1^{+/+}$ OHCs (167 μM; Fig. 8*D*).

To calculate the absolute heights of the energy barriers and to obtain an indication of whether the *Beethoven* mutation affects the rate of entry of DHS molecules into the OHCs, we measured the time constant of the initial decline of the MET current in the presence of the antibiotic (Marcotti et al., 2005). For these experiments, hair bundles were initially deflected toward the inhibitory direction to fully close the MET channel before apply a saturating excitatory mechanical step before and during the extracellular application of different DHS concentrations (Fig. 9*A*,*B*) around the steeper part of the dose–response curves in $Tmc1^{+/+}$ (3 and 30 μM) and $Tmc1^{Bth/Bth}$ (30 and 300 μM; Fig. 7*E*). At the holding potential of −81 mV, DHS caused the MET current to relax to a steady level (Fig. 9*A*,*B*), which reflects the fact that the MET channel has to open first before the block from the antibiotic can occur (open-channel blocker; Marcotti et al., 2005). We then calculated the rate constant k_1 of DHS entry into OHCs (see Materials and Methods) by plotting the inverse of the time constant of DHS binding kinetics (single exponential fits in Fig. 9*A*,*B*) versus its dependence on DHS concentration in both $Tmc1^{+/+}$ and $Tmc1^{Bth/Bth}$ OHCs (Fig. 9*C*); at −81 mV, k_1 was some seven times slower in $Tmc1^{Bth/Bth}$. Figure 9*D* shows that the M412K point mutation reduces the strength of E_b, the DHS binding site in the channel pore, and raises the heights of both energy barriers, but the intracellular barrier E_2 more than the extracellular barrier E_1. The number of DHS molecules entering into the OHCs was estimated as before by assuming a driving force of −150 mV, a total of 80 MET channels per OHC and a resting open probability of the MET channel of 0.3 (Marcotti et al., 2005), but using 1.3 mM extracellular Ca^{2+} as that was how the present experiments were conducted. The result was a substantially reduced entry of DHS molecules in the *Beethoven* mutants ($Tmc1^{+/+}$, 2232/s; $Tmc1^{Bth/Bth}$, 335/s).

Discussion

In this study, we determined that the M412K point mutation in TMC1 of *Beethoven* mice leads to a reduced Ca^{2+} permeability, more so in $Tmc1^{Bth/Bth}$ than in $Tmc1^{Bh/+}$, and conductance of the MET channel of OHCs. We also found that the M412K mutation causes a reduced affinity for the MET channel blocker DHS, which was more pronounced when the aminoglycoside was applied extracellularly. The effects on both Ca^{2+} permeability and DHS block are likely direct consequences of the replacement of a neutral methionine residue by a positively charged lysine affecting the permeation pathway of the channel.

The *Bth* mutation also affects the sensitivity of the MET channel to Ca^{2+} as manifested by the altered shifts in the current-displacement curves on manipulation of extracellular and intracellular Ca^{2+}. In lower vertebrates, these shifts have been interpreted as steady-state manifestations of Ca^{2+}-dependent adaptation (Assad et al., 1989; Crawford et al., 1991; Ricci et al., 1998). Recently, it has been proposed that this is not the case for mammalian cochlear hair cells (Peng et al., 2013), but this view has been challenged on the grounds of technical issues because of glass-probe bundle stimulation (Corns et al., 2014) and underestimation of the Ca^{2+} concentrations that can be reached at the intracellular face of the MET channel (Beurg et al., 2015). In our view, the different effects caused by the *Bth* mutation can be most coherently explained by assuming that it alters Ca^{2+}-dependent adaptation, so that adaptation is stronger than in wild-type controls. Taking 0.04 mM extracellular Ca^{2+} as the reference condition, with little adaptation (Corns et al., 2014), increasing extracellular Ca^{2+} to 0.1 mM induced a stronger rightward adaptive shift in the current-displacement relation of OHCs of *Bth* mutant mice than in controls. Conversely, taking 0.1 mM intracellular BAPTA as the reference for intracellular Ca^{2+} buffering, 3 mM BAPTA was less able to induce a leftward shift in the OHCs of *Bth* mutants. It appears that, in *Bth* mutants, the sensitivity to Ca^{2+} at the sensor for adaptation, which is either part of the intracellular side of the MET channel or positioned very near it (Wu et al., 1999), is, surprisingly, increased, most likely as a downstream compensation mechanism for reduced Ca^{2+} entry through the MET channel. Our findings show that the *Bth* mutation affects Ca^{2+} permeability, the Ca^{2+} and DHS binding site within the channel and Ca^{2+}-dependent adaptation, indicating that TMC1 is a crucial component of the MET channel in hair cells.

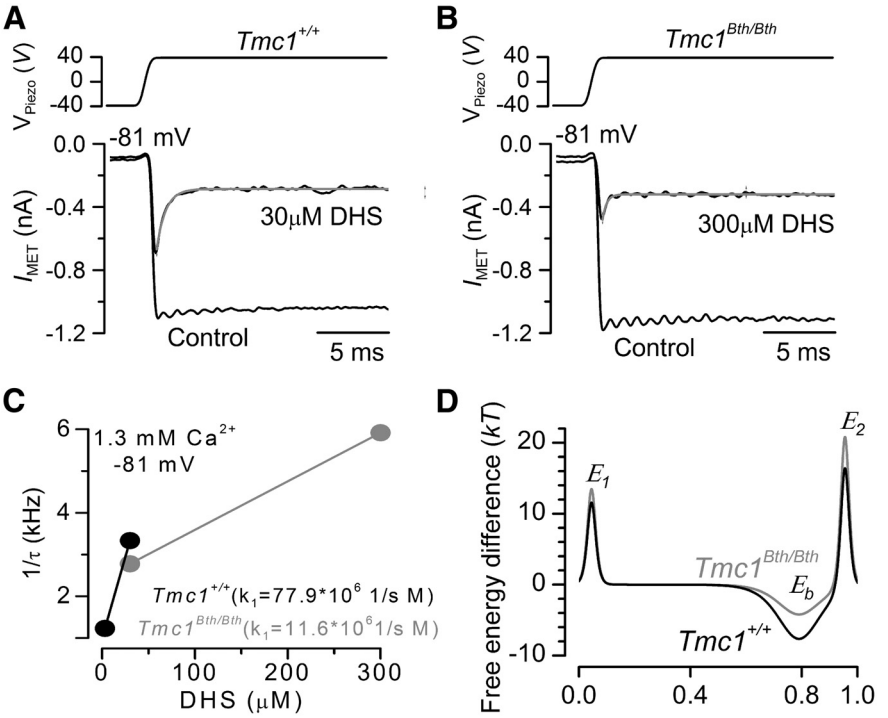

Figure 9. DHS entry into *Beethoven* OHCs. ***A***, ***B***, Block of saturating MET current by extracellular DHS in apical P6 OHCs of $Tmc1^{+/+}$ (***A***) and $Tmc1^{Bth/Bth}$ (***B***) mice in response to step stimuli to the hair bundles (top) and at membrane potentials of −81 mV. MET channels were first closed by inhibitory bundle displacement and then fully opened by an excitatory deflection. Recordings were performed before and during the application of the antibiotic (see Results). The decay of the MET current in the presence of DHS was fitted using a single exponential ($Tmc1^{+/+}$ 30 μM, $\tau = 0.32$ ms; $Tmc1^{Bth/Bth}$ 300 μM, $\tau = 0.14$ ms). ***C***, Rate-constant k_1 was obtained by investigating the DHS-binding kinetics as described previously (Marcotti et al., 2005). The inverse of the time constant of binding ($1/\tau$), which was obtained by the experiments shown in ***A*** and ***B***, was plotted against two different extracellular DHS concentrations in each genotype. Solid lines indicate the fits and the slope k_1 is indicated for both $Tmc1^{+/+}$ and $Tmc1^{Bth/Bth}$ OHCs. ***D***, Energy profiles of two-barrier one-binding-site model for the MET-channel pore of $Tmc1^{+/+}$ (black) and $Tmc1^{Bth/Bth}$ (gray) OHCs. In the absence of a voltage across the membrane ($V_m = 0$), the two barriers have estimated free energies E_1 (11.57 kT for controls and 13.47 kT for *Bth*) and E_2 (16.40 kT for controls and 20.79 kT for *Bth*). The barriers are located at relative electrical distances δ_1 of 0.045 and δ_2 of 0.955, as measured across the membrane from the extracellular side. The two barriers sandwich the binding site for DHS at a relative electrical distance δ_b of 0.79 with a minimum in free energy, E_b of −7.65 *kT* for controls and −4.21 *kT* for *Bth*.

The position of the *Beethoven* mutation

The topology of TMC1 is currently unknown, mainly because the protein is retained in the endoplasmic reticulum (ER) when using in vitro conditions (Kawashima et al., 2011). Using antibodies directed against epitope-tagged versions of the human TMC1 expressed in the ER of heterologous cell lines, TMC1 was predicted to have six transmembrane domains (Labay et al., 2010). If the same transmembrane topology of TMC1 is maintained in the plasma membrane, then the *Bth* M412K point mutation, which is predicted to be in the extracellular loop between the third and fourth membrane spanning domains (Holt et al., 2014), is likely to be located extracellularly. However, the number of transmembrane domains for TMC1 *in vivo* is still unknown, with some algorithms predicting the presence of up to four additional transmembrane regions (Kurima et al., 2002; Keresztes et al., 2003). Therefore, the exact location of M412K will depend on how many of the additional transmembrane domains are present in the native TMC1. Evidence for Tmc1 forming a channel comes from the heterologous expression of a *Caenorhabditis elegans* homolog of *TMC1* (Chatzigeorgiou et al., 2013), which is critical for salt sensation and was inhibited by the stretch-activated channel blocker gadolinium, reported to block the hair cell MET channel (Kimitsuki et al., 1996).

Block of the OHC MET channel by DHS can be described by a two-barrier one-binding-site model with the binding site positioned at a relative electrical distance of 0.79 into the channel from the extracellular side. The binding site is located between

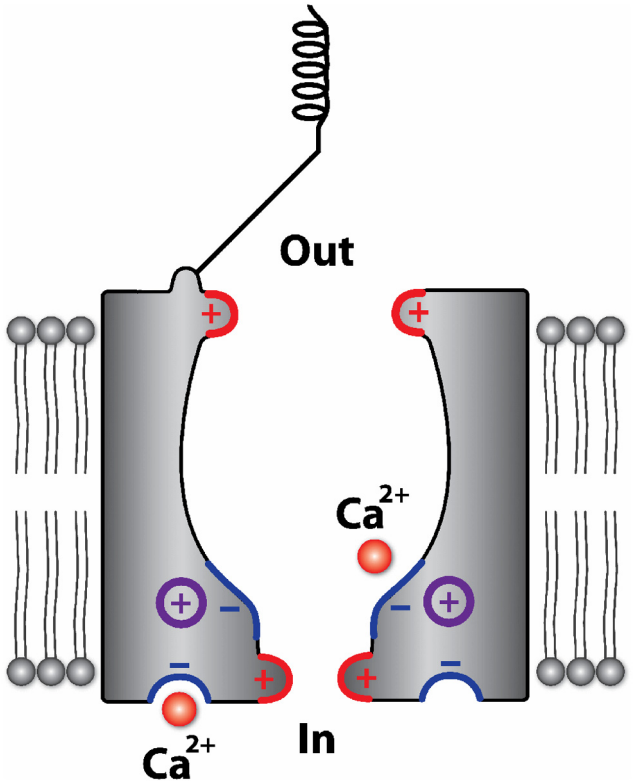

Figure 10. Schematic diagram showing the predicted position of the M412K point mutation in the *Bth* MET channel. Structure of the putative MET channel in hair cells. Both the positively charged extracellular and intracellular barriers (red) and negatively charged DHS (and possibly Ca^{2+}) binding site (blue) are shown. The positively charged TMC1 point mutation (purple) could be present in or close to the pore, near the negatively charged binding site in the vestibule of the channel and the intracellular barrier. The intracellular Ca^{2+} binding site (blue) represents the sensor for adaptation.

two energy barriers, with the intracellular barrier being higher than that on the extracellular side, which accounts in part for the much higher blocking potency of DHS when applied extracellularly (Marcotti et al., 2005; van Netten and Kros, 2007). The presence of a wide channel vestibule facing the extracellular side allows a rapid almost diffusion-limited entry of blockers into its pore region (van Netten and Kros, 2007). The *Beethoven* mutation caused the MET channel to be less sensitive to block by DHS, with a greater reduction occurring when the aminoglycoside was applied extracellularly (7.5-fold) than intracellularly (3.0-fold). The mutation lowered the affinity of the DHS binding site by 3.34 kT. The height of the intracellular energy barrier E_2 was increased by 4.39 kT, hindering movement in either direction of DHS over this barrier, whereas the extracellular barrier E_1 was increased to a lesser extent, by 1.90 kT (Fig. 9). This agrees with the positively charged lysine of the *Bth* mutation most strongly affecting the intracellular side of the channel pore (Fig. 10), near the binding site, at 0.79 electrical distance, and the intracellular barrier. This lysine is thus likely to be present in or near the permeation pore of the MET channel, in which it reduces the affinity of DHS for a binding site for polycations deep in the vestibule of the channel, near the selectivity filter of the narrow pore region (Van Netten and Kros, 2007).

It is interesting to compare the reduced affinity for DHS of OHCs of *Bth* mutant mice with the anomalous MET currents recorded from cochlear hair cells of mice that have no tip-link-gated MET channels (Marcotti et al., 2014), in which the K_D was, at 894 μM, eight times higher than in the $Tmc1^{Bth/Bth}$ OHCs. There, it was proposed that the vestibule, and hence the polycationic binding site, was lacking. Together, our findings strengthen the evidence for TMC1 being an integral component of the MET channel (Holt et al., 2014). In the mechanosensitive channel Piezo1, an E2133K point mutation (replacing a negatively charged glutamate with a positive lysine) similarly reduced its Ca^{2+} permeability and the blocking potency of the polycationic ruthenium red, leading to the conclusion that this residue must be at or near the pore (Coste et al., 2015).

Functional consequences of the *Beethoven* mutation

The size of the MET currents in *Beethoven* mutant OHCs is normal at least until around the onset of hearing, and yet compound action potential (CAP) responses are absent in young mice (Marcotti et al., 2006). This suggests that a more subtle defect is responsible for the progressive hearing loss phenotype in the *Beethoven* mutant mice (Vreugde et al., 2002; Marcotti et al., 2006). Recently, it has been proposed that the reduced expression of the plasma membrane Ca^{2+} ATPase 2 (PMCA2) pump in the stereociliary bundle of *Beethoven* OHCs could contribute to the hearing loss (Beurg et al., 2015). Defects in PMCA2 have been linked to deafness in mice (Street et al., 1998; Bortolozzi et al., 2010) and associated with reductions in endocochlear potential (Wood et al., 2004) and endolymphatic Ca^{2+}, which would disrupt the PCDH15–cadherin 23 interaction at the tip link (Kazmierczak et al., 2007). However, given that both endocochlear potential (Marcotti et al., 2006) and MET current size (Fig. 1) in *Beethoven* mice were normal, reduced PMCA2 is unlikely to contribute significantly to the hearing phenotype in *Bth* mutants.

We propose that the stronger MET current adaptation is the main causative factor of the hearing loss. The hair bundles of the immature mouse cochlea OHCs are exposed to an *in vivo* endolymphatic Ca^{2+} concentration of $\leq$0.3 mM but higher than the 0.04 mM in the mature cochlea (Johnson et al., 2012). Despite the reduced Ca^{2+} influx into the MET channel of *Bth* mutants, the channel is kept in a more strongly adapted state, already evident at 0.1 mM Ca^{2+}, which results in a lower fraction of the current activated at the resting bundle position. The reduced resting open probability of the immature hair bundle of *Bth* mutant OHCs will reduce the standing inward MET current and cause their membrane potential (V_m) to hyperpolarize compared with control cells (approximately −40 mV; Johnson et al., 2011). The similarity between our findings in OHCs and those reported previously in IHCs (Pan et al., 2013) suggests that the *Bth* mutation is also likely to hyperpolarize the IHC resting V_m (approximately −60 mV; Johnson et al., 2011). Alteration of the normal electrical activity in developing cochlear hair cells has been associated with defects in the synaptic machinery and basolateral membrane properties (Roux et al., 2009; Johnson et al., 2013), which resemble those observed in the *Bth* mutant hair cells (Marcotti et al., 2006). The reduced expression of the potassium current $I_{K,n}$ from approximately P8 onward in OHCs (Vreugde et al., 2002; Marcotti et al., 2006) is likely to contribute to the hearing defects observed in young and adult mice (Marcotti et al., 2006). Although *Bth* mutant OHCs retain their characteristic electromotile activity (Marcotti et al., 2006), the shift in their V_m will affect the optimal activation of the motor protein prestin (Ashmore, 2008; Johnson et al., 2011), which drives electromotility (He et al., 1994; Marcotti and Kros, 1999).

References

Ashmore J (2008) Cochlear outer hair cell motility. Physiol Rev 88:173–210. CrossRef Medline

Assad JA, Hacohen N, Corey DP (1989) Voltage dependence of adaptation and active bundle movement in bullfrog saccular hair cells. Proc Natl Acad Sci U S A 86:2918–2922. CrossRef Medline

Assad JA, Shepherd GM, Corey DP (1991) Tip-link integrity and mechanical transduction in vertebrate hair cells. Neuron 7:985–994. CrossRef Medline

Beurg M, Fettiplace R, Nam JH, Ricci AJ (2009) Localization of inner hair cell mechanotransducer channels using high-speed calcium imaging. Nat Neurosci 12:553–558. CrossRef Medline

Beurg M, Kim KX, Fettiplace R (2014) Conductance and block of hair-cell mechanotransducer channels in transmembrane channel-like protein mutants. J Gen Physiol 144:55–69. CrossRef Medline

Beurg M, Goldring AC, Fettiplace R (2015) The effects of *Tmc1 Beethoven* mutation on mechanotransducer channel function in cochlear hair cells. J Gen Physiol 146:233–243. CrossRef Medline

Bortolozzi M, Brini M, Parkinson N, Crispino G, Scimemi P, De Siati RD, Di Leva F, Parker A, Ortolano S, Arslan E, Brown SD, Carafoli E, Mammano F (2010) The novel PMCA2 pump mutation Tommy impairs cytosolic calcium clearance in hair cells and links to deafness in mice. J Biol Chem 285:37693–37703. CrossRef Medline

Bosher SK, Warren RL (1978) Very low calcium content of cochlear endolymph, an extracellular fluid. Nature 273:377–378. CrossRef Medline

Chatzigeorgiou M, Bang S, Hwang SW, Schafer WR (2013) tmc-1 encodes a sodium-sensitive channel required for salt chemosensation in *C. elegans*. Nature 494:95–99. CrossRef Medline

Corns LF, Johnson SL, Kros CJ, Marcotti W (2014) Calcium entry into stereocilia drives adaptation of the mechanoelectrical transducer current of mammalian cochlear hair cells. Proc Natl Acad Sci U S A 111:14918–14923. CrossRef Medline

Coste B, Murthy SE, Mathur J, Schmidt M, Mechioukhi Y, Delmas P, Patapoutian A (2015) Piezo1 ion channel pore properties are dictated by C-terminal region. Nat Commun 6:7223. CrossRef Medline

Crawford AC, Evans MG, Fettiplace R (1991) The actions of calcium on the mechano electrical transducer current of turtle hair cells. J Physiol 434:369–398. CrossRef Medline

Goodyear RJ, Marcotti W, Kros CJ, Richardson GP (2005) Development and properties of stereociliary link types in hair cells of the mouse cochlea. J Comp Neurol 485:75–85. CrossRef Medline

He DZ, Evans BN, Dallos P (1994) First appearance and development of electromotility in neonatal gerbil outer hair cells. Hear Res 78:77–90. CrossRef Medline

Holt JR, Pan B, Koussa MA, Asai Y (2014) TMC function in hair cell transduction. Hear Res 311:17–24. CrossRef Medline

Johnson SL, Beurg M, Marcotti W, Fettiplace R (2011) Prestin-driven cochlear amplification is not limited by the outer hair cell membrane time constant. Neuron 70:1143–1154. CrossRef Medline

Johnson SL, Kennedy HJ, Holley MC, Fettiplace R, Marcotti W (2012) The resting transducer current drives spontaneous activity in pre-hearing mammalian cochlear inner hair cells. J Neurosci 32:10479–10483. CrossRef Medline

Johnson SL, Kuhn S, Franz C, Ingham N, Furness DN, Knipper M, Steel KP, Adelman JP, Holley MC, Marcotti W (2013) Presynaptic maturation in auditory hair cells requires a critical period of sensory-independent spiking activity. Proc Natl Acad Sci U S A 110:8720–8725. CrossRef Medline

Kawashima Y, Géléoc GS, Kurima K, Labay V, Lelli A, Asai Y, Makishima T, Wu DK, Della Santina CC, Holt JR, Griffith AJ (2011) Mechanotransduction in mouse inner ear hair cells requires transmembrane channel-like genes. J Clin Invest 121:4796–4809. CrossRef Medline

Kazmierczak P, Sakaguchi H, Tokita J, Wilson-Kubalek EM, Milligan RA, Müller U, Kachar B (2007) Cadherin 23 and protocadherin 15 interact to form tip-link filaments in sensory hair cells. Nature 449:87–91. CrossRef Medline

Keresztes G, Mutai H, Heller S (2003) TMC and EVER genes belong to a larger novel family, the TMC gene family encoding transmembrane proteins. BMC Genomics 4:24. CrossRef Medline

Kimitsuki T, Nakagawa T, Hisashi K, Komune S, Komiyama S (1996) Gadolinium blocks mechano-electric transducer current in chick cochlear hair cells. Hear Res 101:75–80. CrossRef Medline

Kroese AB, Das A, Hudspeth AJ (1989) Blockage of the transduction channels of hair cells in the bullfrog's sacculus by aminoglycoside antibiotics. Hear Res 37:203–217. CrossRef Medline

Kros CJ, Rüsch A, Richardson GP (1992) Mechano-electrical transducer currents in hair cells of the cultured neonatal mouse cochlea. Proc Biol Sci 249:185–193. CrossRef Medline

Kurima K, Peters LM, Yang Y, Riazuddin S, Ahmed ZM, Naz S, Arnaud D, Drury S, Mo J, Makishima T, Ghosh M, Menon PS, Deshmukh D, Oddoux C, Ostrer H, Khan S, Riazuddin S, Deininger PL, Hampton LL, Sullivan SL, Battey JF Jr, Keats BJ, Wilcox ER, Friedman TB, Griffith AJ (2002) Dominant and recessive deafness caused by mutations of a novel gene, TMC1, required for cochlear hair-cell function. Nat Genet 30:277–284. CrossRef Medline

Kurima K, Ebrahim S, Pan B, Sedlacek M, Sengupta P, Millis BA, Cui R, Nakanishi H, Fujikawa T, Kawashima Y, Choi BY, Monahan K, Holt JR, Griffith AJ, Kachar B (2015) TMC1 and TMC2 localize at the site of mechanotransduction in mammalian inner ear hair cell stereocilia. Cell Rep 12:1606–1617. CrossRef Medline

Labay V, Weichert RM, Makishima T, Griffith AJ (2010) Topology of transmembrane channel-like gene 1 protein. Biochemistry 49:8592–8598. CrossRef Medline

Marcotti W, Kros CJ (1999) Developmental expression of the potassium current IK, N contributes to maturation of the mouse outer hair cells. J Physiol 520:653–660. CrossRef Medline

Marcotti W, van Netten SM, Kros CJ (2005) The aminoglycoside antibiotic dihydrostreptomycin rapidly enters hair cells through the mechano-electrical transducer channels. J Physiol 567:505–521. CrossRef Medline

Marcotti W, Erven A, Johnson SL, Steel KP, Kros CJ (2006) Tmc1 is necessary for normal functional maturation and survival of inner and outer hair cells in the mouse cochlea. J Physiol 574:677–698. CrossRef Medline

Marcotti W, Corns LF, Desmonds T, Kirkwood NK, Richardson GP, Kros CJ (2014) Transduction without tip links in cochlear hair cells is mediated by ion channels with permeation properties distinct from those of the mechano-electrical transducer channel. J Neurosci 34:5505–5514. CrossRef Medline

Nakanishi H, Kurima K, Kawashima Y, Griffith AJ (2014) Mutations of TMC1 cause deafness by disrupting mechanoelectrical transduction. Auris Nasus Larynx 41:399–408. CrossRef Medline

Nam JH, Peng AW, Ricci AJ (2015) Underestimated sensitivity of mammalian cochlear hair cells due to splay between stereociliary columns. Biophys J 108:2633–2647. CrossRef Medline

Ohmori H (1985) Mechano-electrical transduction currents in isolated vestibular hair cells of the chick. J Physiol 359:189–217. CrossRef Medline

Pan B, Géléoc GS, Asai Y, Horwitz GC, Kurima K, Ishikawa K, Kawashima Y, Griffith AJ, Holt JR (2013) TMC1 and TMC2 are components of the mechanotransduction channel in hair cells of the mammalian inner ear. Neuron 79:504–515. CrossRef Medline

Partanen JI (2010) Re-evaluation of the thermodynamic activity quantities in aqueous rubidium and cesium chloride solutions at 25°C. J Chem Eng Data 55:249–257. CrossRef

Peng AW, Effertz T, Ricci AJ (2013) Adaptation of mammalian auditory hair cell mechanotransduction is independent of calcium entry. Neuron 80:960–972. CrossRef Medline

Pickles JO, Comis SD, Osborne MP (1984) Cross-links between stereocilia in the guinea pig organ of Corti, and their possible relation to sensory transduction. Hear Res 15:103–112. CrossRef Medline

Rard JA, Clegg SL (1997) Critical evaluation of the thermodynamic properties of aqueous calcium chloride. 1. Osmotic and activity coefficients of 0–10.77 mol.kg^{-1} aqueous calcium chloride solutions at 298.15 K and correlation with extended pitzer ion-interaction models. J Chem Eng Data 42:819–849. CrossRef

Ricci A (2002) Differences in mechano-transducer channel kinetics underlie tonotopic distribution of fast adaptation in auditory hair cells. J Neurophysiol 87:1738–1748. Medline

Ricci AJ, Fettiplace R (1998) Calcium permeation of the turtle hair cell mechanotransducer channel and its relation to the composition of endolymph. J Physiol 506:159–173. CrossRef Medline

Ricci AJ, Wu YC, Fettiplace R (1998) The endogenous calcium buffer and the time course of transducer adaptation in auditory hair cells. J Neurosci 18:8261–8277. Medline

Roux I, Hosie S, Johnson SL, Bahloul A, Cayet N, Nouaille S, Kros CJ, Petit C, Safieddine S (2009) Myosin VI is required for the proper maturation and function of inner hair cell ribbon synapses. Hum Mol Genet 18:4615–4628. CrossRef Medline

Salt AN, Inamura N, Thalmann R, Vora A (1989) Calcium gradients in inner ear endolymph. Am J Otolaryngol 10:371–375. CrossRef Medline

Street VA, McKee-Johnson JW, Fonseca RC, Tempel BL, Noben-Trauth K (1998) Mutations in a plasma membrane Ca^{2+}-ATPase gene cause deafness in deafwaddler mice. Nat Genet 19:390–394. CrossRef Medline

van Netten SM, Kros CJ (2007) Insights into the pore of the hair cell transducer channel from experiments with permeant blockers. Curr Top Membr 59:375–398. CrossRef Medline

Vreugde S, Erven A, Kros CJ, Marcotti W, Fuchs H, Kurima K, Wilcox ER, Friedman TB, Griffith AJ, Balling R, Hrabé De Angelis M, Avraham KB, Steel KP (2002) Beethoven, a mouse model for dominant, progressive hearing loss DFNA36. Nat Genet 30:257–258. CrossRef Medline

Wood JD, Muchinsky SJ, Filoteo AG, Penniston JT, Tempel BL (2004) Low endolymph calcium concentrations in deafwaddler2J mice suggest that PMCA2 contributes to endolymph calcium maintenance. J Assoc Res Otolaryngol 5:99–110. Medline

Wu YC, Ricci AJ, Fettiplace R (1999) Two components of transducer adaptation in auditory hair cells. J Neurophysiol 82:2171–2181. Medline

Xiong W, Grillet N, Elledge HM, Wagner TF, Zhao B, Johnson KR, Kazmierczak P, Müller U (2012) TMHS is an integral component of the mechanotransduction machinery of cochlear hair cells. Cell 151:1283–1295. CrossRef Medline

Zhao B, Wu Z, Grillet N, Yan L, Xiong W, Harkins-Perry S, Müller U (2014) TMIE is an essential component of the mechanotransduction machinery of cochlear hair cells. Neuron 84:954–967. CrossRef Medline